geodiversitas

2026 • 48 • 3

A new kentriodontid dolphin (Cetacea, Odontoceti, Delphinida) from the Middle Miocene of the southeastern Pacific

Olivier LAMBERT, Maëlle OBERLIN, Christian de MUIZON, Alberto COLLARETA, Mario URBINA & Giovanni BIANUCCI

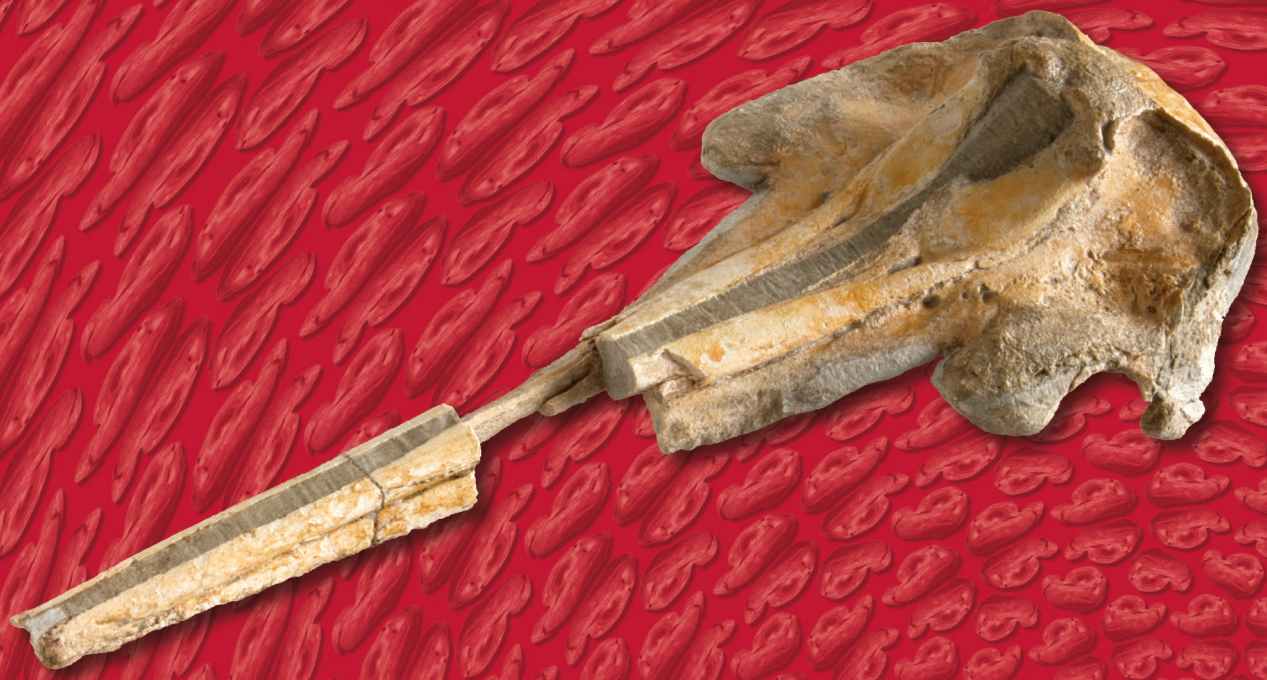

art. 48 (3) — Published on 19 February 2026
www.geodiversitas.com

PUBLICATIONS SCIENTIFIQUES

MUSÉUM NAL HIST NATURELLE

Geodiversitas est indexé dans / Geodiversitas *is indexed in:*
– Science Citation Index Expanded (SciSearch®)
– ISI Alerting Services®
– Current Contents® / Physical, Chemical, and Earth Sciences®
– Scopus®

Geodiversitas est distribué en version électronique par / Geodiversitas *is distributed electronically by:*
– BioOne® (http://www.bioone.org)

Les articles ainsi que les nouveautés nomenclaturales publiés dans *Geodiversitas* sont référencés par / *Articles and nomenclatural novelties published in* Geodiversitas *are referenced by:*
– ZooBank® (http://zoobank.org)

Geodiversitas est une revue en flux continu publiée par les Publications scientifiques du Muséum, Paris
Geodiversitas *is a fast track journal published by the Museum Science Press, Paris*

Les Publications scientifiques du Muséum publient aussi / *The Museum Science Press also publish:* ***Adansonia***, ***Zoosystema***, ***Anthropozoologica***, ***European Journal of Taxonomy***, ***Naturae***, ***Cryptogamie*** **sous-sections** ***Algologie***, ***Bryologie***, ***Mycologie, Comptes Rendus Palevol***

Diffusion – Publications scientifiques Muséum national d'Histoire naturelle
CP 41 – 57 rue Cuvier F-75231 Paris cedex 05 (France)
Tél. : 33 (0)1 40 79 48 05 / Fax : 33 (0)1 40 79 38 40
diff.pub@mnhn.fr / http://sciencepress.mnhn.fr

ISSN (imprimé / *print*) : 1280-9659/ ISSN (électronique / *electronic*) : 1638-9395

A new kentriodontid dolphin (Cetacea, Odontoceti, Delphinida) from the Middle Miocene of the southeastern Pacific

Olivier LAMBERT
D.O. Terre et Histoire de la Vie, Institut royal des Sciences naturelles de Belgique,
29 rue Vautier, B-1000 Brussels (Belgium)
olambert@naturalsciences.be (corresponding author)

Maëlle OBERLIN
Université de Strasbourg, CNRS, IPHC UMR 7178, F-67000 Strasbourg (France)
and Centre d'Études biologiques de Chizé, CNRS, UMR 7372, F-79360 Villiers en Bois (France)
maelle.oberlin.pro@gmail.com

Christian de MUIZON
CR2P (CNRS, MNHN, Sorbonne Université), Département Origines et Évolution,
Muséum national d'Histoire naturelle, case postale 38, 57 rue Cuvier, F-75231 Paris cedex 05 (France)
muizon@mnhn.fr

Alberto COLLARETA
Dipartimento di Scienze della Terra, Università di Pisa, via S. Maria 53, I-56126 Pisa (Italy)
alberto.collareta@unipi.it

Mario URBINA
Departamento de Paleontología de Vertebrados, Museo de Historia Natural-Universidad Nacional
Mayor de San Marcos, Avenida Arenales 1256, P-15072 Lima (Peru)
mariourbina01@hotmail.com

Giovanni BIANUCCI
Dipartimento di Scienze della Terra, Università di Pisa, via S. Maria 53, I-56126 Pisa (Italy)
giovanni.bianucci@unipi.it

Submitted on 27 March 2025 | accepted on 13 May 2025 | published on 19 February 2026

urn:lsid:zoobank.org:pub:6DFFE442-7DE6-42CF-B184-5B94B354FB36

Lambert O., Oberlin M., Muizon C. de, Collareta A., Urbina M. & Bianucci G. 2026. — A new kentriodontid dolphin (Cetacea, Odontoceti, Delphinida) from the Middle Miocene of the southeastern Pacific. *Geodiversitas* 48 (3): 25-50. https://doi.org/10.5252/geodiversitas2026v48a3. http://geodiversitas.com/48/3

ABSTRACT
The origin of most modern families of dolphins and porpoises has to be found during the Early to Middle Miocene, presumably among the stock of early delphinidan forms generally attributed to the family Kentriodontidae Slijper, 1936. The East Pisco Basin (Peru) is a major source of Miocene odontocetes (echolocating toothed cetaceans), but up to now a majority of the finds originate from the Lower Miocene Chilcatay Formation and the Upper Miocene deposits of the Pisco Formation. Apart from the poorly known early delphinidan *Incacetus broggii* Colbert, 1944, very little is known for the Middle Miocene layers of the Pisco Formation. Based on a sample of three skulls collected from the Langhian to Serravallian (14.7-12.6 Ma) P0 allomember of the Pisco Formation in two locali-

ties (Santa Rosa and Mal Paso) of the East Pisco Basin, we describe a new genus and species of early delphinidan, *Mesokentriodon protohumboldti* n. gen., n. sp. Characterized by a moderately elongated rostrum and 40 teeth per upper row, this medium-sized dolphin shares many cranial similarities with, among others, the smaller *Kentriodon pernix* Kellogg, 1927, the type species of the type genus of the family Kentriodontidae. As our phylogenetic analyses consistently recover the new taxon in a clade that also includes *K. pernix*, we confidently identify it as a kentriodontid, though the content of this family varies considerably across the various analyses using different implied weighting protocols. Our favoured hypothesis is that kentriodontids are stem-group delphinidans whose chronostratigraphic distribution fills a major Early to Middle Miocene time interval before the appearance of the earliest members of the extant delphinidan lineages (Lipotidae Zhou, Qian & Li, 1978, Inioidea Muizon, 1988, and Delphinoidea Gray, 1821). This new species improves the relatively poor Middle Miocene fossil record of cetaceans in the East Pisco Basin and highlights the potential of the lower portion of the Pisco Formation for enhancing our understanding of the emergence of the modern delphinidan clades.

KEY WORDS
Odontoceti,
Delphinida,
Kentriodontidae,
East Pisco Basin,
Pisco Formation,
Miocene,
Langhian,
Serravallian,
phylogeny,
new genus,
new species.

RÉSUMÉ
Un nouveau dauphin kentriodontidé (Cetacea, Odontoceti, Delphinida) du Miocène moyen du Pacifique sud-est.
L'origine de la plupart des familles modernes de dauphins et de marsouins est à rechercher au Miocène inférieur à moyen, vraisemblablement parmi le stock de formes de premiers Delphinida Muizon, 1984 généralement attribuées à la famille Kentriodontidae Slijper, 1936. Le bassin de Pisco (Pérou) est une source majeure d'odontocètes (cétacés à dents) du Miocène, mais jusqu'à présent, la majorité des découvertes proviennent du Miocène inférieur de la Formation Chilcatay et des dépôts du Miocène supérieur de la Formation Pisco. À l'exception du Delphinida ancien mal connu *Incacetus broggii* Colbert, 1944, on sait très peu de choses sur les couches du Miocène moyen de la Formation Pisco. Sur la base d'un échantillon de trois crânes collectés dans l'allomembre P0 de la Formation Pisco, daté du Langhien au Serravallien (14,7-12,6 Ma), dans deux localités (Santa Rosa et Mal Paso) du bassin de Pisco est, nous décrivons un nouveau genre et une nouvelle espèce de Delphinida, *Mesokentriodon protohumboldti* n. gen., n. sp. Caractérisé par un rostre modérément allongé et 40 dents par rangée supérieure, ce dauphin de taille moyenne partage de nombreuses similitudes crâniennes avec, entre autres, le plus petit *Kentriodon pernix* Kellogg, 1927, l'espèce type du genre type de la famille Kentriodontidae. Comme nos analyses phylogénétiques retrouvent systématiquement le nouveau taxon dans un clade qui inclut également *K. pernix*, nous l'identifions avec confiance comme un kentriodontidé, bien que le contenu de cette famille varie considérablement selon les diverses analyses utilisant différents protocoles de pondération implicite. Notre hypothèse privilégiée est que les kentriodontidés sont des Delphinida du groupe souche dont la distribution chronostratigraphique remplit un intervalle de temps majeur du Miocène inférieur au Miocène moyen, avant l'apparition des premiers membres des lignées de Delphinida modernes (Lipotidae Zhou, Qian & Li, 1978, Inioidea Muizon, 1988, et Delphinoidea Gray, 1821). Cette nouvelle espèce améliore le registre fossile relativement pauvre des cétacés du Miocène moyen dans le bassin de Pisco est, et met en évidence le potentiel de la partie inférieure de la Formation Pisco pour améliorer notre compréhension de l'émergence des clades de Delphinida modernes.

MOTS CLÉS
Odontoceti,
Delphinida,
Kentriodontidae,
bassin de Pisco est,
Formation Pisco,
Miocène,
Langhien,
Serravallien,
phylogénie,
genre nouveau,
espèce nouvelle.

INTRODUCTION

Delphinida is a large clade of odontocetes (echolocating toothed whales) including most extant families of dolphins and porpoises (with the exception of Platanistidae) and totalling more than 50 modern species (Würsig *et al.* 2018; Committee on Taxonomy 2024). While late Oligocene records remain to be fully assessed, the origin of this clade can be more firmly traced back to the Early Miocene, with the earliest members of the family Kentriodontidae (Ichishima *et al.* 1995; Marx *et al.* 2016; Nobile *et al.* 2024). Kentriodontids are the only delphinidans known from Lower to Middle Miocene deposits, prior to the emergence of the first members of several modern delphinidan families in Late Miocene times (e.g., Murakami *et al.* 2014; Lambert *et al.* 2021; Kimura & Hasegawa 2024). Despite a recent increase in published works on the subject, the phylogenetic relationships of kentriodontids remain highly debated and complex: this family is often considered as non-monophyletic, and some of its members have variably been recovered in different cladistic analyses as stem delphinidans, stem delphinoids, or even as sister-group to the lipotids and/or inioids (Muizon 1988b; Lambert *et al.* 2017; Peredo *et al.* 2018; Guo & Kohno 2023). Nevertheless, with their worldwide distribution and broad range of body sizes and cranial morphologies (from small to large size dolphins, with varying rostral proportions and tooth counts), kentriodontids are a testament to the first major delphinidan radiation (True 1912; Kellogg 1927; Rensberger 1969; Barnes 1978; Muizon 1988a; Ichishima 1995; Dawson 1996; Bianucci 2001; Kazár 2005; Lambert *et al.* 2005; Salinas-Márquez *et al.* 2014; Godfrey & Lambert 2023; Kimura & Hasegawa 2019).

Located along the southern coast of Peru, the East Pisco Basin yielded a moderately rich record of early delphinidans. While the oldest such finds originate from the Burdigalian of the Chilcatay Formation (many specimens of *Kentriodon* sp.; Bianucci *et al.* 2018), the bulk of this record is from the overlying Pisco Formation. The best-known Pisco species, the small-sized *Atocetus iquensis*, is based on several well-preserved specimens including subcomplete skulls and ear bones, from basal layers of the P2 allomember (upper Tortonian) at the locality of Cerro la Bruja; the longirostrine *Belonodelphis peruanus* is more fragmentarily known, as the holotype and only specimen includes a partial cranium and mandible, the periotics, a fragmentary tympanic bulla, and some vertebrae, and it originates from either the base of P2 or the top of P1 (upper Tortonian), at the same Cerro la Bruja locality as *A. iquensis*; similarly based on a poorly preserved holotype, comprising a very damaged skull with ear bones, vertebrae, ribs, part of the sternum, and limb bones, the somewhat larger *Incacetus broggii* is thought to originate from the P0 allomember (upper Langhian to Serravallian) (Colbert 1944; Muizon 1988a; Ochoa *et al.* 2021; Bianucci & Collareta 2022). The geographic origin of the latter species was traced back by CdM to the locality of Santa Rosa (Fig. 1), where in 1987 he collected the remains of a small cetotheriid baleen whale as well as two crania of a medium-sized early delphinidan (Muizon 1988a; Marx *et al.* 2017). Another skull with associated ear bones belonging to the same delphinidan form was subsequently collected from P0 strata at the locality of Mal Paso.

In this work, we describe these three odontocete specimens, compare them to other early delphinidans worldwide and analyse their phylogenetic relationships, thus contributing to improving the knowledge on the first radiation(s) of these ancient relatives of nowadays' dolphins and porpoises.

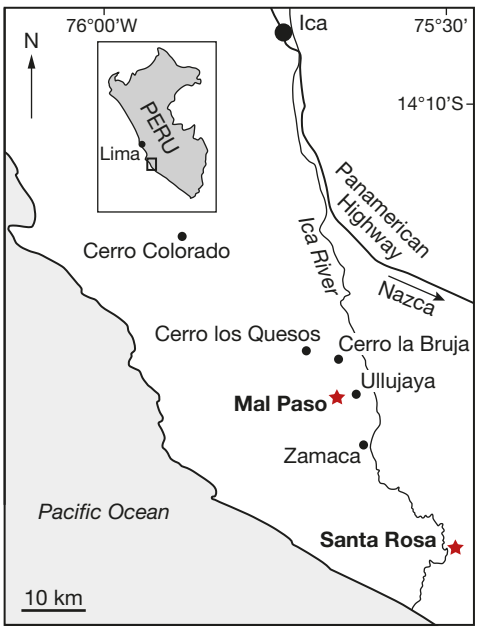

Fig. 1. — Schematic map of the East Pisco Basin, modified from Marx *et al.* (2017), showing the localities (**red stars**) where specimens of *Mesokentriodon protohumboldti* n. gen., n. sp. were collected: Mal Paso for the referred specimen MUSM4693 and Santa Rosa for both the holotype MNHN.F.PPI282 and the paratype MNHN.F.PPI283. Inset: schematic map of Peru with the position of the East Pisco Basin.

MATERIAL AND METHODS

Institutional abbreviations

AMNH	American Museum of Natural History, New York;
CMM	Calvert Marine Museum, Solomons;
IRSNB	Institut royal des Sciences naturelles de Belgique, Brussels;
LACM	Natural History Museum of Los Angeles County, Los Angeles;
MNHN	Muséum national d'Histoire naturelle, Paris;
MUSM	Museo de Historia Natural de la Universidad Nacional Mayor de San Marcos, Lima;
USNM	National Museum of Natural History, Smithsonian Institution, Washington, D.C.

Anatomical and taxonomic terminology

The terminology for cranial anatomy follows Mead & Fordyce (2009), except when explicitly stated. As detailed farther in the text, the family Kentriodontidae is restricted here to a clade including taxa more closely related to *Kentriodon pernix* than to other delphinidan families. Other early delphinidans from the Miocene that do not fall in any well-defined family are cited as either 'kentriodontids' s.l. or early delphinidans.

Phylogenetic analyses

To investigate the phylogenetic relationships of the studied taxon, we modified the character-taxon matrix of Bianucci *et al.* (2022) with the addition of the new genus and species described here, totalling 374 characters and 149 taxa (Appendices 1-2). The parsimony analyses were performed with PAUP version 4.0 (Swofford 2003). *Bos taurus*, *Hippopotamus amphibius*, and *Sus scrofa* were selected as outgroups. A constraint tree from Bayesian analysis of molecular data (McGowen *et al.* 2009, 2011; Geisler *et al.* 2011; Appendix 3) was used as a backbone to force relationships among extant cetaceans. The heuristic searches were performed with simple taxon addition, a tree-bisection-reconnection algorithm, and ACCTRAN optimization. Several heuristic searches were undertaken under equal and implied weights, using for the latter different values for K (3, 6, 9, and 12). Bootstrap and jackknife analyses using 100 replicates were run with the same settings as the ones yielding our two preferred trees.

SYSTEMATIC PALAEONTOLOGY

Order CETACEA Brisson, 1762
Clade PELAGICETI Uhen, 2008
Clade NEOCETI Fordyce & Muizon, 2001
Suborder ODONTOCETI Flower, 1867

Infraorder DELPHINIDA Muizon, 1984
Family KENTRIODONTIDAE Slijper, 1936

COMMENT

The content of the family Kentriodontidae remains in flux (see discussion below). We opt here for a pragmatic solution, this clade being restricted to *Kentriodon pernix*, the type species of the type genus for this family, and all other early delphinidans more closely related to the former than to other delphinidan families (Lipotidae Zhou, Qian & Li, 1978, Iniidae Gray, 1846, Pontoporiidae Gray, 1870, Albireonidae Barnes, 1984, Odobenocetopsidae Muizon, 1993, Monodontidae Gray, 1821, Phocoenidae Gray, 1825, and Delphinidae Gray, 1821). In all our phylogenetic analyses (see 'Phylogenetic analysis' below), the new genus and species described herein is recovered in this clade, and it can thus be identified as a kentriodontid.

As we failed to consistently recover any subfamilies (or families in the superfamily Kentriodontoidea) as supported instead by previous studies (e.g., Barnes 1978; Muizon 1988b; Guo & Kohno 2023), we do not further comment on the definition and content of such subclades, following on that matter Lambert *et al.* (2017) and Peredo *et al.* (2018).

Genus *Mesokentriodon* n. gen.

urn:lsid:zoobank.org:act:4303C2FE-40A9-4DEA-917C-C980F24F9A0E

TYPE AND ONLY SPECIES. — *Mesokentriodon protohumboldti* n. gen., n. sp.

ETYMOLOGY. — 'meso' from Ancient Greek μέσος, intermediate, and 'kentriodon' for the type genus of the family Kentriodontidae, the new genus and species described here being intermediate in size between e.g. the smaller *Kentriodon pernix* and the larger *Macrokentriodon morani*.

DIAGNOSIS. — As for the type species.

Mesokentriodon protohumboldti n. sp.
(Figs 2-13; Tables 1; 2; Appendices 1-5)

urn:lsid:zoobank.org:act:5F4D65A5-BA8F-4008-BFBB-EE855D670BBA

TYPE MATERIAL. — **Holotype**. **Peru** • 1 specimen (a subcomplete cranium lacking part of the right orbit, part of the basicranium, the ear bones, and teeth); East Pisco Basin, Santa Rosa locality; 14°47'22.9"S, 75°30'22.5"W; Pisco Formation, P0 allomember; Langhian to Serravallian (Middle Miocene); VII.1978; C. de Muizon leg.; MNHN[MNHN.F.PPI282].
Paratype. **Peru** • 1 specimen (a cranium lacking parts of a 55 mm-long section of the rostrum, part of the palate, of the basicranium, and of the occipital shield, as well as all the ear bones and teeth); same data as for the holotype; MNHN[MNHN.F.PPI283].

TYPE LOCALITY. — Santa Rosa, East Pisco Basin, Peru; approximate geographic coordinates: 14°47'22.9"S, 75°30'22.5"W (Fig. 1). This is the type locality of the cetotheriid mysticete *Tiucetus rosae* (Marx *et al.* 2017) and, possibly, the early delphinidan *Incacetus broggii* (Colbert 1944; Muizon 1988a).

TYPE HORIZON AND AGE. — Pisco Formation, P0 allomember, including the Santa Rosa vertebrate level (Muizon 1988a). The P0 allomember constitutes the lowest unit of the Pisco Formation (Di Celma *et al.* 2017; Bosio *et al.* 2020b). Once poorly constrained to a broad interval between 18 and 9.5 Ma (Bosio *et al.* 2020a), it is now dated to the Middle Miocene (Langhian to Serravallian) by means of Strontium Isotope ($^{87}Sr/^{86}Sr$) Stratigraphy on mollusk and barnacle shells, carbonate nodules, and shark teeth (yielding an age of 14.7-12.6 Ma at the site of Mal Paso; Bosio *et al.* 2020a; 2022), as well as through diatom biostratigraphy (yielding an age of 14.2-12.9 Ma at the site of Cerro Tiza; Malinverno *et al.* 2025).

OTHER REFERRED SPECIMEN. — **Peru** • 1 specimen (skull including the highly damaged cranium and left mandible, the subcomplete left periotic, part of the left tympanic bulla, and teeth); East Pisco Basin, Mal Paso locality (Fig. 1); 14°34'49.1"S, 75°40'10.4"W; Pisco Formation, P0 allomember; Langhian to Serravallian (Middle Miocene); MUSM [MUSM4693].
This specimen was illustrated on site with field number MLP5 in Collareta *et al.* (2021b: fig. 4G, H). See also DeVries *et al.* (2006), Di Celma *et al.* (2017), and Collareta *et al.* (2021a, 2023) for stratigraphic and palaeontological information on the Mal Paso locality.

ETYMOLOGY. — 'proto' from Ancient Grek πρωτο (first, before) and 'humboldti' for the Humboldt Current, flowing along the western coast of South America. The Middle Miocene strata of the Pisco Formation from where the new species originates have been proposed to precede the full establishment of the Humboldt Current Ecosystem in this region (see Bosio *et al.* 2020b; Collareta *et al.* 2021b).

DIAGNOSIS. — With a bizygomatic width ranging between more than 164 mm and 200 mm, this medium-sized early delphinidan can be distinguished from other Miocene delphinidan species generally placed in the family Kentriodontidae by the following unique combination of characters: moderately elongated rostrum making about 67 % of condylobasal length; 40 teeth per upper row (37 maxillary teeth and 3 premaxillary teeth); diameter of maxillary alveoli ranging between 5.5 and 7.0 mm at mid-length of rostrum; broad dorsal opening of mesorostral groove along whole rostrum; width of dorsal exposure of maxilla at rostrum base subequal to width of premaxilla at the same level; V-shaped antorbital notch drawing angle of 45-50°; rounded ventral outline of preorbital region; vertical and slender postorbital process of frontal; premaxillary foramen located at level of the antorbital notches; at least three dorsal infraorbital foramina per side in antorbital region; presphenoid not reaching dorsally level of anteromedial edge of premaxillary sac fossa; pterygoid sinus fossa extending anterior to level of antorbital notches; well-defined fossa in frontal for postorbital lobe of pterygoid sinus; convex dorsal outline of vertex in lateral view; deep vertical notch along anterior margin of nasal; anterolateral projection of nasal anteriorly longer than anteromedial tip; moderately deep internasal fossa; maximum length of frontal on vertex shorter than maximum length of nasal; absence of contact between premaxilla and frontal on vertex; posterior part of vertex transversely broader than bony nares; short but well-defined external occipital crest; temporal fossa slightly longer than high, with roof of fossa reaching dorsal level intermediate between those of orbit and vertex; well-defined anterodorsal angle on anterior process of periotic more posterior than anteroventral tip thereof; broad anterior incisure; tear drop-shaped internal auditory meatus; much reduced superior process of the periotic (nearly absent in medial view); and poorly posteriorly extended posterior process of the periotic (posterodorsal margin making an angle of about 110° with long axis of bone in lateral view). See below for a more detailed comparisons with nominal species of early delphinidans from the Miocene.

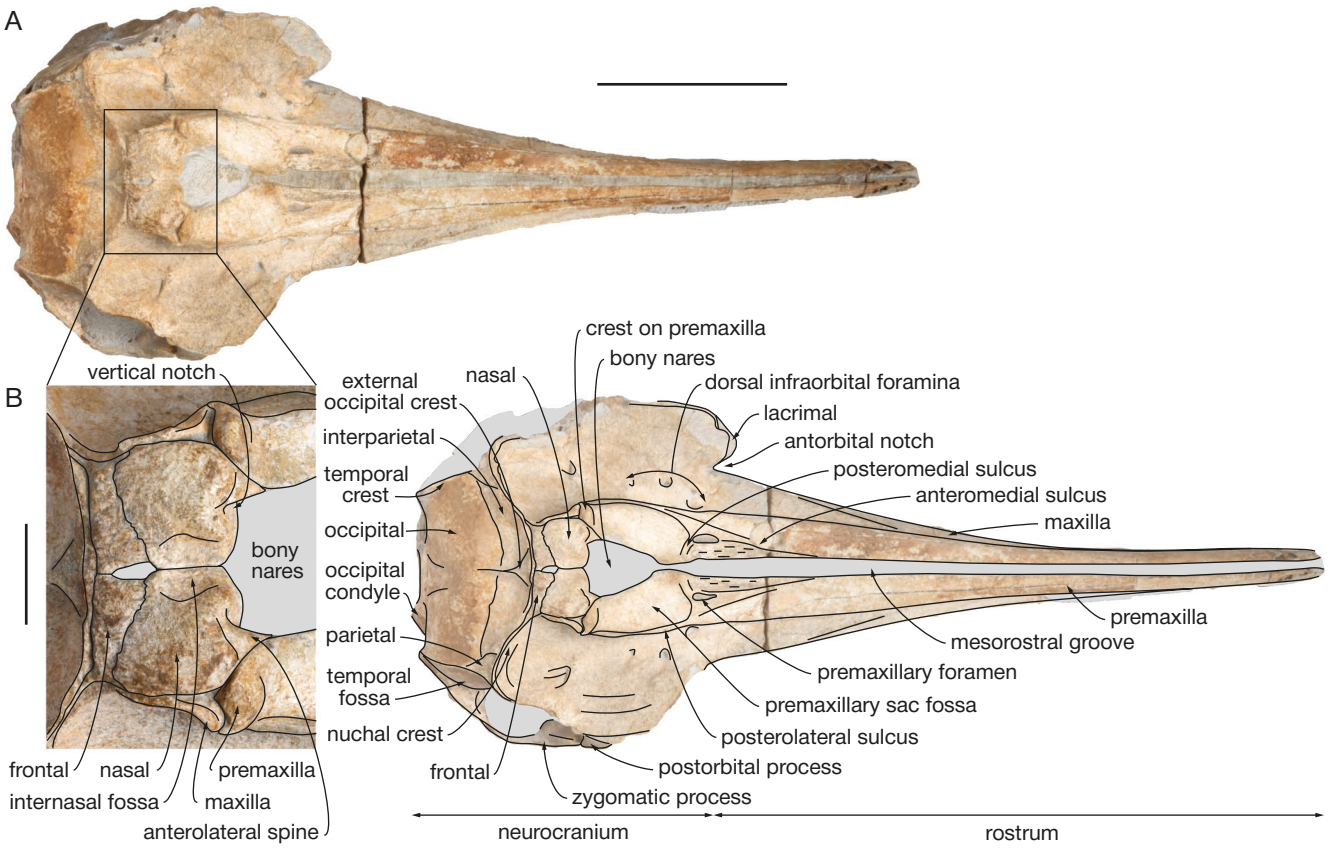

Fig. 2. — Cranium of *Mesokentriodon protohumboldti* n. gen., n. sp. MNHN.F.PPI282 (holotype) in dorsal view (**A**) with explanatory line drawing and detail of the vertex in dorsal view (**B**). **Grey shading** for hardened sediment. Scale bars: A, 100 mm; B, 20 mm. Photos: Olivier Lambert.

Anatomical description

The description of the cranium is mostly based on MNHN.F.PPI282 (holotype) and MNHN.F.PPI283 (paratype), the two best-preserved specimens. Both crania lack some parts of the orbits, palate, and basicranium, and some regions could not be fully prepared due to the combination of a hardened entombing sediment and fractured and/or very delicate underlying bones. Combining elements of the right and left sides of these two specimens allows for the description of nearly all cranial parts, except for some missing portions of the pterygoids, of the basioccipital, and of the exoccipitals, as well as the ear bones and teeth, which are only preserved in MUSM4693. In turn, the cranium and mandible of the latter specimen are much more damaged. Consequently, only cranial measurements are provided herein for MUSM4693, together with the detailed description of the periotic, the partial tympanic, and one detached tooth. Very similar cranial dimension (Table 1) and cranial morphology strongly support the referral of this specimen to the species *Mesokentriodon protohumboldti* n. gen., n. sp.

Ontogenetic stage

None of the three studied specimens preserves postcranial parts, hence the lack of information on the degree of vertebral epiphyseal fusion. The three crania display robust and well-ossified bones, as well as well-defined dental alveoli, and we could not find any indication of fully open cranial sutures, though the suture lines of the interparietal with the parietals and occipital remain visible in the holotype (see below). Cranial dimensions are generally slightly smaller in the paratype, compared to the two other specimens (Table 1), but no clues for an earlier ontogenetic stage could be found. The detached tooth associated to MUSM4693 does not display any significant apical wear and its pulp cavity is nearly closed by dentine. All things considered the three specimens are interpreted as representing subadult to adult individuals (Perrin 1975; Perrin & Myrick 1980).

General morphology of the cranium

Bizygomatic width ranges between more than 164 mm and 200 mm, corresponding to an odontocete in the cranial size range of the modern common dolphin, *Delphinus delphis*. The rostrum is moderately elongated, making 66-67.5 % of the condylobasal length (Table 1), a ratio falling within the 'longirostrine' category of McCurry & Pyenson (2019). While the cross section of the rostrum at mid-length is as high as wide in both the holotype and the paratype, the anterior tip of the rostrum is slightly wider in the paratype. The mesorostral groove is broadly dorsally open (though slightly less so in the holotype and MUSM4693), with the maximum opening being located a short distance anterior to

TABLE 1. — Cranial measurements (in mm) of *Mesokentriodon protohumboldti* n. gen., n. sp. MNHN.F.PPI282, MNHN.F.PPI283, and MUSM4693. Abbreviations: **+**, incomplete; **e**, estimate; **–**, no data; (**r**), right side, (**l**), left side.

	MNHN.F.PPI282 (holotype)	MNHN.F.PPI283 (paratype)	MUSM 4693
condylobasal length	+480	+440	+417
rostrum length	324	292	+279
width of rostrum at mid-length	33	29	–
height of rostrum at mid-length	33.5	29	–
width of premaxillae at rostrum mid-length	27	24	–
distance from rostrum tip to anterior end of palatine	286	253	–
length of upper alveolar row	286(l)/288(r)	264(r)	–
number of upper alveoli per row	40	–	–
distance between last left and right maxillary alveoli	66	60	–
maximum width of dorsal opening of mesorostral groove	10.5	13	11
distance between premaxillae at anterior margin of bony nares	3	5	e4.5
width of rostrum at base	e104	91	104
height of rostrum at base	48	44	–
width of premaxillae at rostrum base	59	47	53.5
width of right premaxilla at rostrum base	24.5	19.5	e24.5
width of left premaxilla at rostrum base	25	21.5	e22
preorbital width	+174	164.5	e182
postorbital width	e182	+161	e196
bizygomatic width	e186	+164	e200
maximum width of premaxillae in facial region	70.5	61	66
width of right premaxillary sac fossa	33	28	–
width of left premaxillary sac fossa	33	31.5	–
orbit length (left)	e57	e54.5	e54
anteroposterior length of temporal fossa (left)	89	–	86
dorsoventral height of temporal fossa	67	e65	e70
maximum width of bony nares	29	27	e27
minimum width across ascending processes of premaxillae	63.5	56	–
maximum width of premaxillae at anterior margin of vertex	66	61	–
maximum width of nasals	49	44.5	–
maximum length of nasals	33	+24	–
length of median suture between nasals	15	e11	–
minimum distance between maxillae across vertex	43	36	e35
minimum distance between temporal crests across occipital shield	78.5	–	77.5
distance between anterior tip of zygomatic process and ventral tip of postglenoid process	59.5	+55	e50
width of mandibular fossa	26	–	–
width of occipital condyles	e74	–	–
left periotic total length	–	–	+24.8
left periotic mediolateral width	–	–	17.8
left periotic dorsoventral thickness	–	–	10.8
length of anterior process of left periotic	–	–	7.3
length of pars cochlearis of left periotic (from anterior margin to anterior margin of fenestra rotunda)	–	–	9.1
dorsoventral thickness of pars cochlearis (from anterior margin to medial margin of internal acoustic meatus)	–	–	8.7
distance between fenestra rotunda and tip of anterior process	–	–	16.8
distance between distal opening of facial canal and tip of anterior process	–	–	12.9
maximum dorsoventral thickness of involucrum of left tympanic bulla (in anterior half)	–	–	8.6

the level of the antorbital notches, at about the anterior tip of the anteromedial sulcus (Figs 2, 3, 10A). In lateral view the ventral margin of the rostrum is convex for most of its length, while the dorsal margin is roughly rectilinear. Only complete in the holotype, the upper alveolar series include 40 alveoli each (Fig. 6). In lateral view, the facial region is moderately concave, with a gradual rise (that is somewhat steeper in the holotype) towards the vertex (Figs 4, 5, 10B). The vertex is located at about the same anteroposterior level as the postorbital process. Medial sutures between the bones exposed at the vertex (i.e., nasals and frontals) are situated along the midline (a character best seen in the holotype), and the right and left premaxillary sac fossae are either equal or subequal in width, thus implying little to no facial asymmetry. The minimum transverse width of the vertex is observed across the frontals; it is greater than the width of the bony nares. The temporal fossa is only slightly longer than high, with the roof reaching a dorsal level intermediate between those of the orbit and vertex in the three specimens. Making the posterior edge of the temporal fossa, the nuchal crest extends behind the posterior surface of the occipital shield. The nuchal and temporal crests are modestly developed, i.e., low and thin in cross section. Both the occipital shield and the medial wall of the temporal fossa are convex, thus testifying to an inflated endocranial cavity.

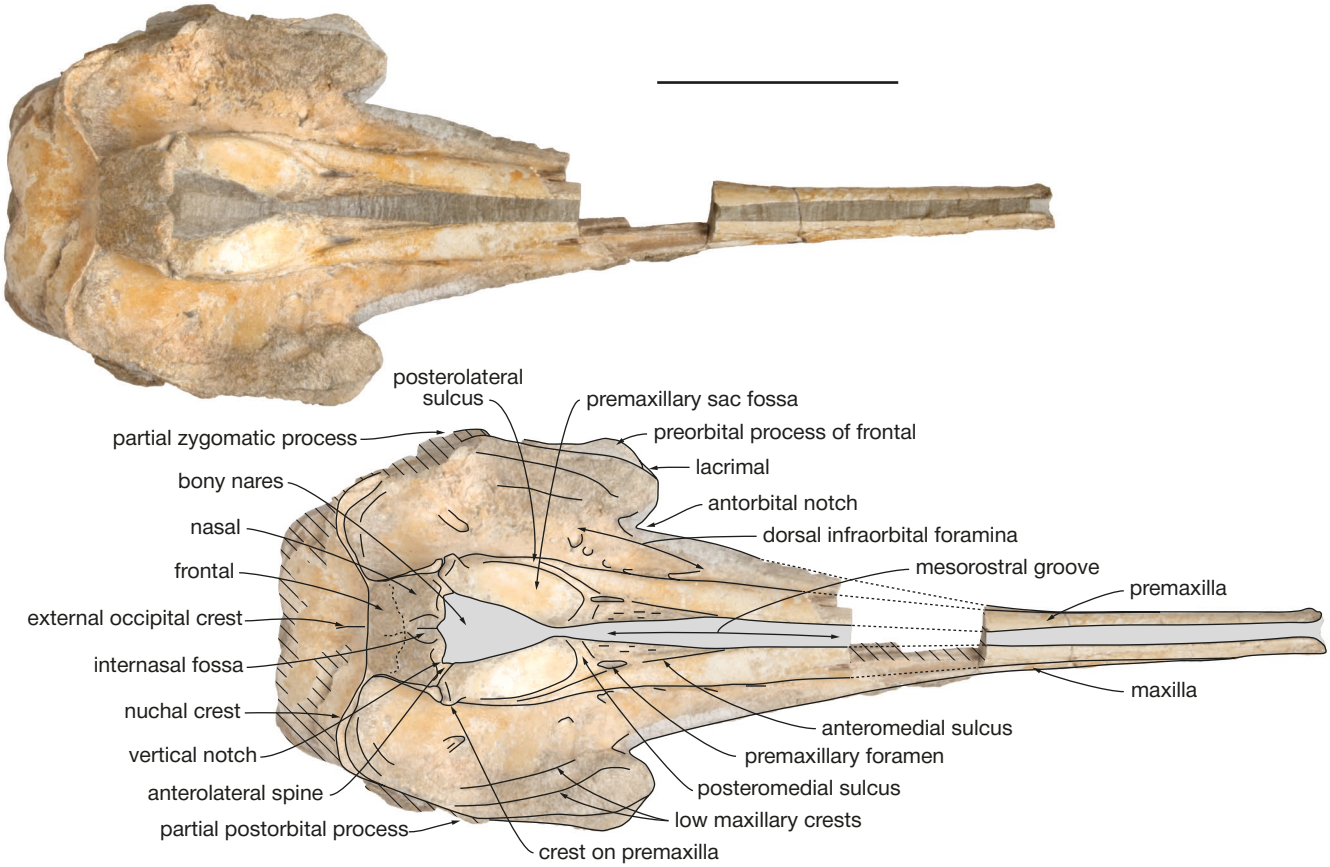

Fig. 3. — Cranium of *Mesokentriodon protohumboldti* n. gen., n. sp. MNHN.F.PPI283 (paratype) in dorsal view with explanatory line drawing. **Grey shading** for hardened sediment; **hatching** for main break surfaces; **dashed lines** for more tentative interpretations of sutures and edges. Scale bar: 100 mm.

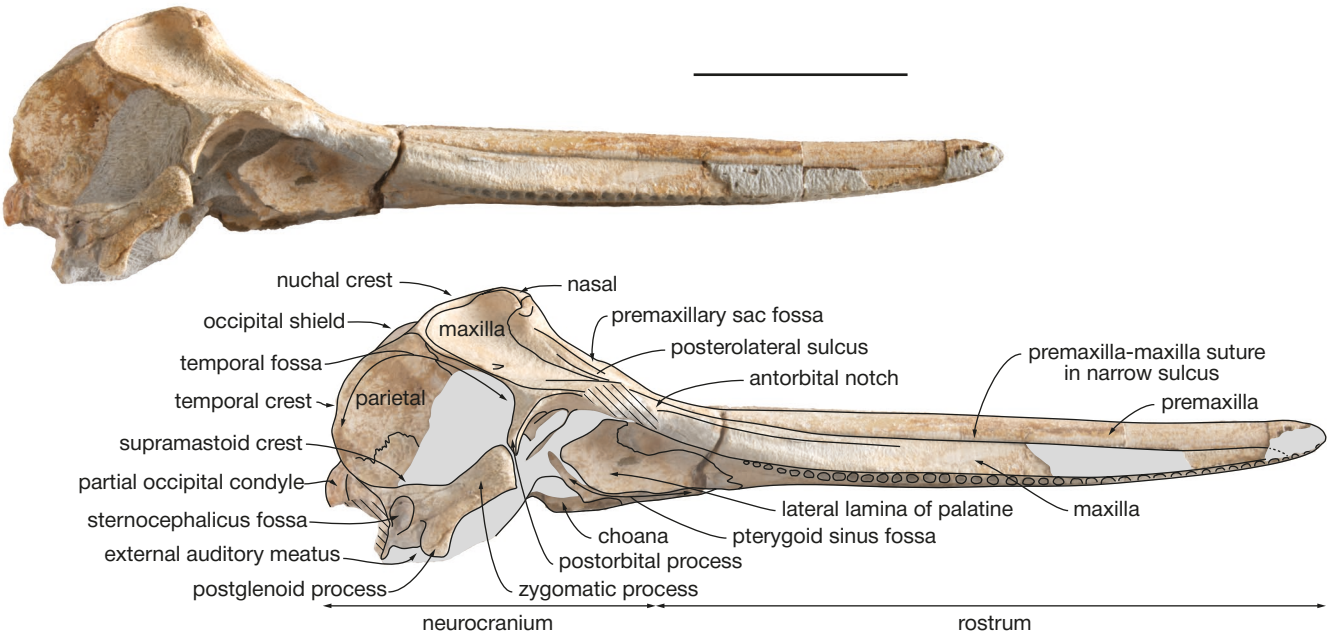

Fig. 4. — Cranium of *Mesokentriodon protohumboldti* n. gen., n. sp. MNHN.F.PPI282 (holotype) in right lateral view with explanatory line drawing. **Grey shading** for hardened sediment; **hatching** for main break surfaces; **dashed lines** for more tentative interpretations of sutures. Scale bar: 100 mm. Photos: Olivier Lambert.

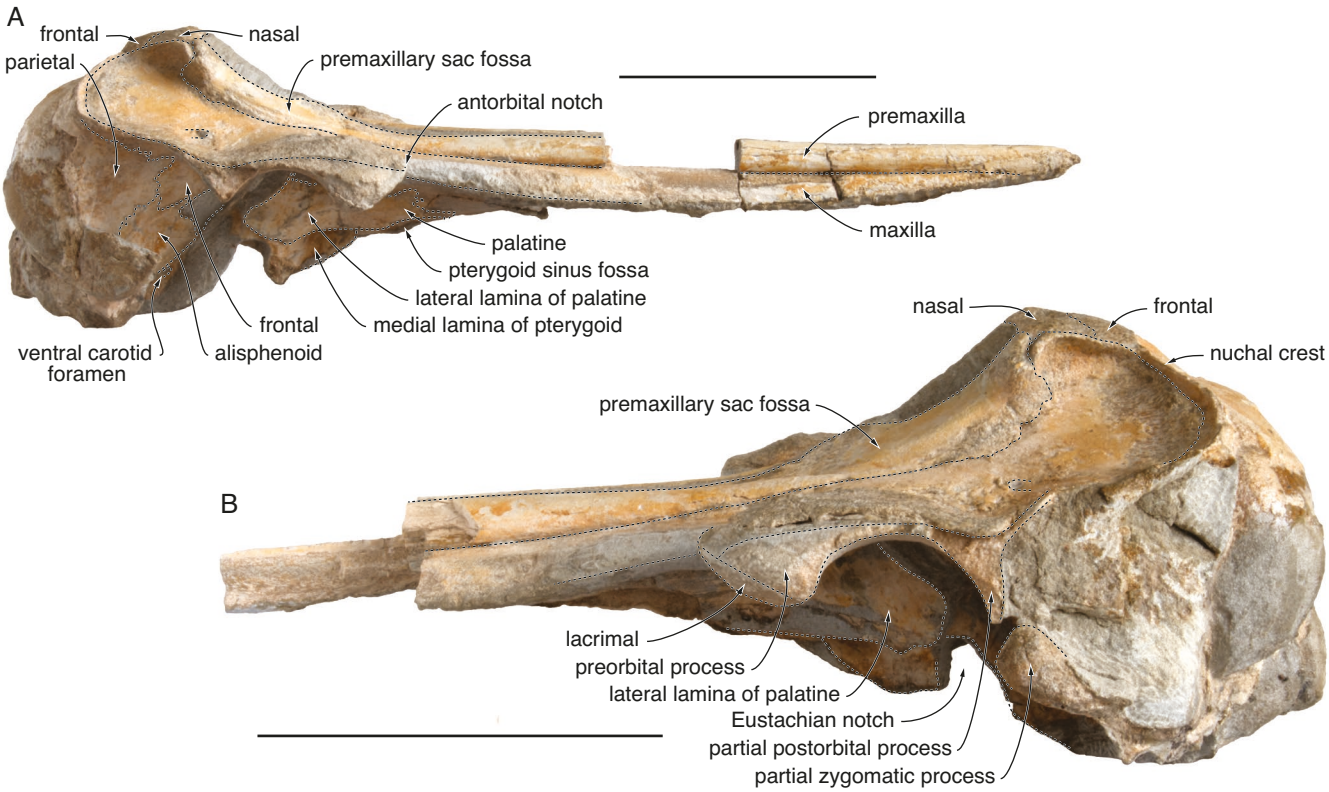

Fig. 5. — Cranium of *Mesokentriodon protohumboldti* n. gen., n. sp. MNHN.F.PPI283 (paratype) in right (**A**) and left (**B**, without the anterior part of the rostrum) lateral view. **Dashed lines** for main sutures and bone edges. Scale bars: 100 mm. Photos: Olivier Lambert.

Premaxilla

The anterior apex of the rostrum is comprised of the premaxillae alone. The maxilla-premaxilla suture can be followed on the left side of the holotype until 22 mm posterior to the tip of the rostrum, where it turns abruptly ventrally. Only three upper alveoli are found in the premaxilla. The first premaxillary alveolus is only slightly larger than the two others, a feature best seen in the paratype, where the outline of the tip of the rostrum in ventral view is more rectangular than in the holotype. This first alveolus is directed more anteriorly than the others, being possibly subhorizontal in both the holotype and paratype (though alveolar walls are too poorly preserved for a precise assessment of the direction). The first upper incisor may thus have been procumbent, but without reaching the size of the apical upper tusks seen in the holotype of *Kentriodon pernix* (Kellogg 1927).

Along the lateral surface of the rostrum, the maxilla-premaxilla suture runs into a narrow sulcus, which broadens locally at levels where a small dorsal infraorbital foramen is probably present (though covered by sediment) and followed anteriorly by a larger sulcus (Figs 4; 5). In dorsal view, the premaxilla is wider than the maxilla before the level of the antorbital notch (Figs 2; 3, 10A). At this level, both bones are subequal in width in the holotype and MUSM4693, while the right premaxilla is narrower than the right maxilla in the paratype, making about 75 per cent of the width of the latter. At the level of the antorbital notch, the lateral margin of each premaxilla is only slightly constricted in correspondence to a main dorsal infraorbital foramen that pierces the adjacent maxilla just lateral to the premaxilla-maxilla suture (see below). The transversely narrow premaxillary foramen (13 mm-long in the holotype) is also located at this anteroposterior level in the three specimens. The 40 mm-long anteromedial sulcus laterally defines a transversely concave prenarial triangle with an irregular surface ornamented by thin longitudinal crests and grooves. The broad and well-defined posteromedial sulcus raises obliquely towards the markedly elevated anteromedial edge of the premaxillary sac fossa. Right and left anteromedial edges are at a short distance to each other (more so in the holotype, see Table 1), nearly completely closing the U-shaped bony nares anteromedially. Each premaxillary sac fossa is only slightly concave transversely, a feature that is locally accentuated by the elevation of the medial edge thereof. Each fossa is also only slightly concave anteroposteriorly. The dorsal surface of the fossa is elevated compared to the lateral suture with the maxilla, being separated from the latter by a 7 to 11 mm-high lateral wall. Best developed in the holotype, this wall is excavated by a shallow posterolateral sulcus that vanishes at about mid-length of the bony nares. The lateral margin of the ascending process of the premaxilla is constricted before thickening laterally and anterodorsally to form a transversely directed (in dorsal view) and lateroventrally sloping (in anterior view) small crest (Figs 2-3). This crest shortly overhangs the more ventral part of the bone in all the specimens, being reminiscent of the transversely directed

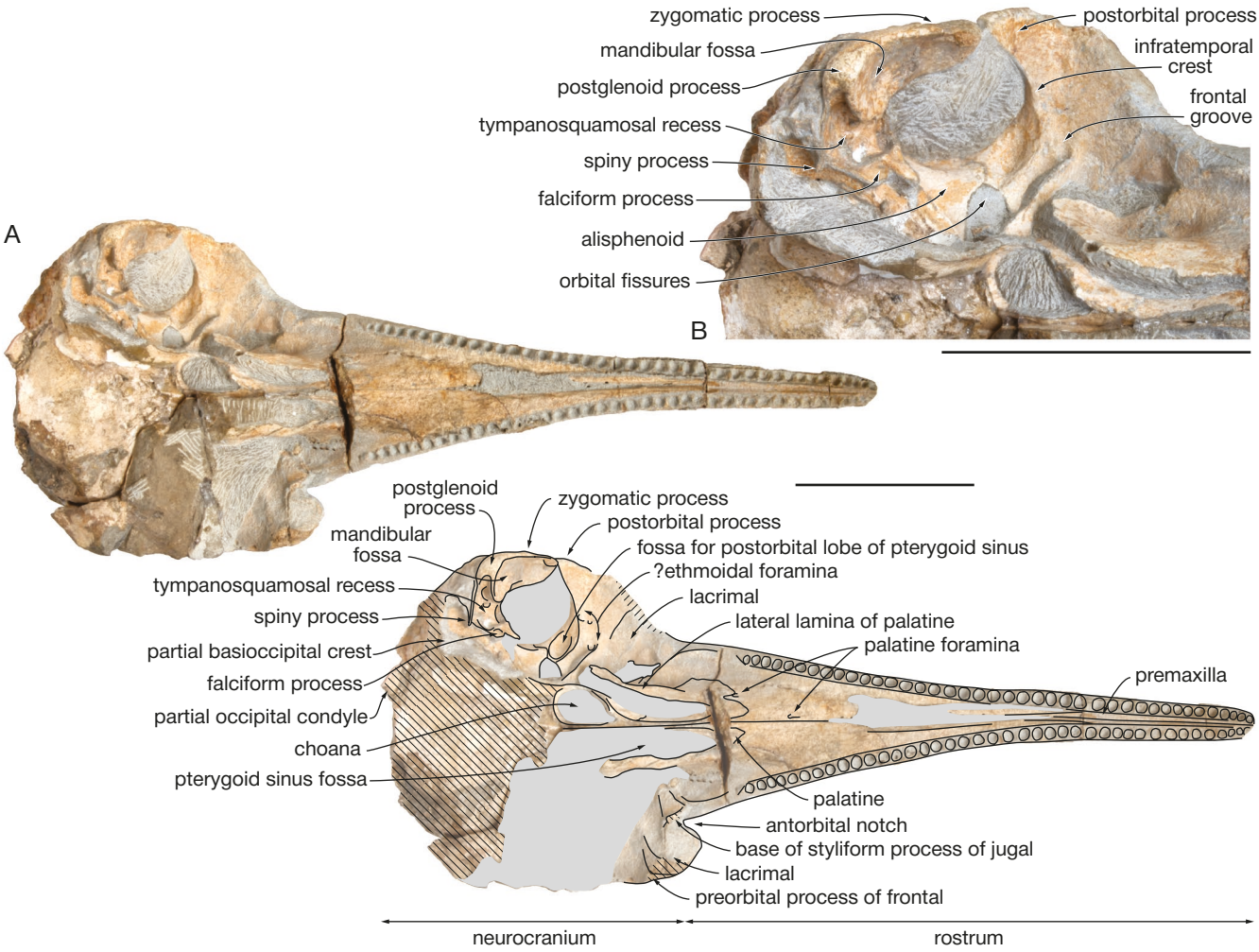

Fig. 6. — Cranium of *Mesokentriodon protohumboldti* n. gen., n. sp. MNHN.F.PPI282 (holotype) in ventral view (**A**) with explanatory line drawing and detail of right side of basicranium and palate in ventral view (**B**). **Grey shading** for hardened sediment; **hatching** for main break surfaces. Scale bars: 100 mm. Photos: Olivier Lambert.

premaxillary crest in some ziphiids (e.g., the modern *Berardius* spp.). This crest broadly contacts the anterolateral margin of the nasal. It is separated from the high medial edge of the maxilla along the vertex by a curved, deep, and narrow sulcus. A transverse line joining the blunt posterior ends of the right and left premaxillae is at the same anteroposterior level as the posteromedial edge of the bony nares.

Maxilla

The lateral margin of the maxilla is made of spongy bone in the region just anterior to the antorbital notch, making the distinction between bone and hardened sediment – and as such, mechanical preparation of the fossil – locally challenging. The outline of the maxillary flange is therefore difficult to describe; it is interpreted as somewhat laterally convex, dorsoventrally thick, and only little elevated dorsally compared to the slightly transversely concave more median region of the maxilla. The antorbital notch is deep (12-15 mm) and V-shaped in the three specimens, drawing an angle of 45°-50° in dorsal view (Figs 2, 3, 10A). Several small dorsal infraorbital foramina (at least two on each side in the holotype and at least three on the right side and two on the left in the paratype) open anteriorly just lateral to the maxilla-premaxilla suture in the posterior third of the rostrum. A major dorsal infraorbital foramen (diameter ranging between 5 and 7 mm) opens anteriorly to anterolaterally on each side of the holotype and paratype, at about the same level as the premaxillary foramen, at a very short distance (1.5 to 2 mm) from the maxilla-premaxilla suture. A second large foramen (diameter ranging between 4 and 6 mm) is located posterolaterally on both sides of MNHN.F.PPI282 and MNHN.F.PPI283, and it opens laterally. On the left side of the paratype, a smaller (diameter of 3 mm) foramen is observed between the two main foramina, while the holotype also includes a smaller (2 to 2.5 mm) foramen, but posterior to the second main foramen, seen on both maxillae. The posteriormost dorsal infraorbital foramen is found at the center of the ascending process, posterior to the level of the postorbital process. Its diameter ranges from 5 to 7.5 mm, and the broad sulcus that leaves posterolaterally from this foramen is partly bisected by a shallow crest on the right side of both the holotype and paratype. The dorsal

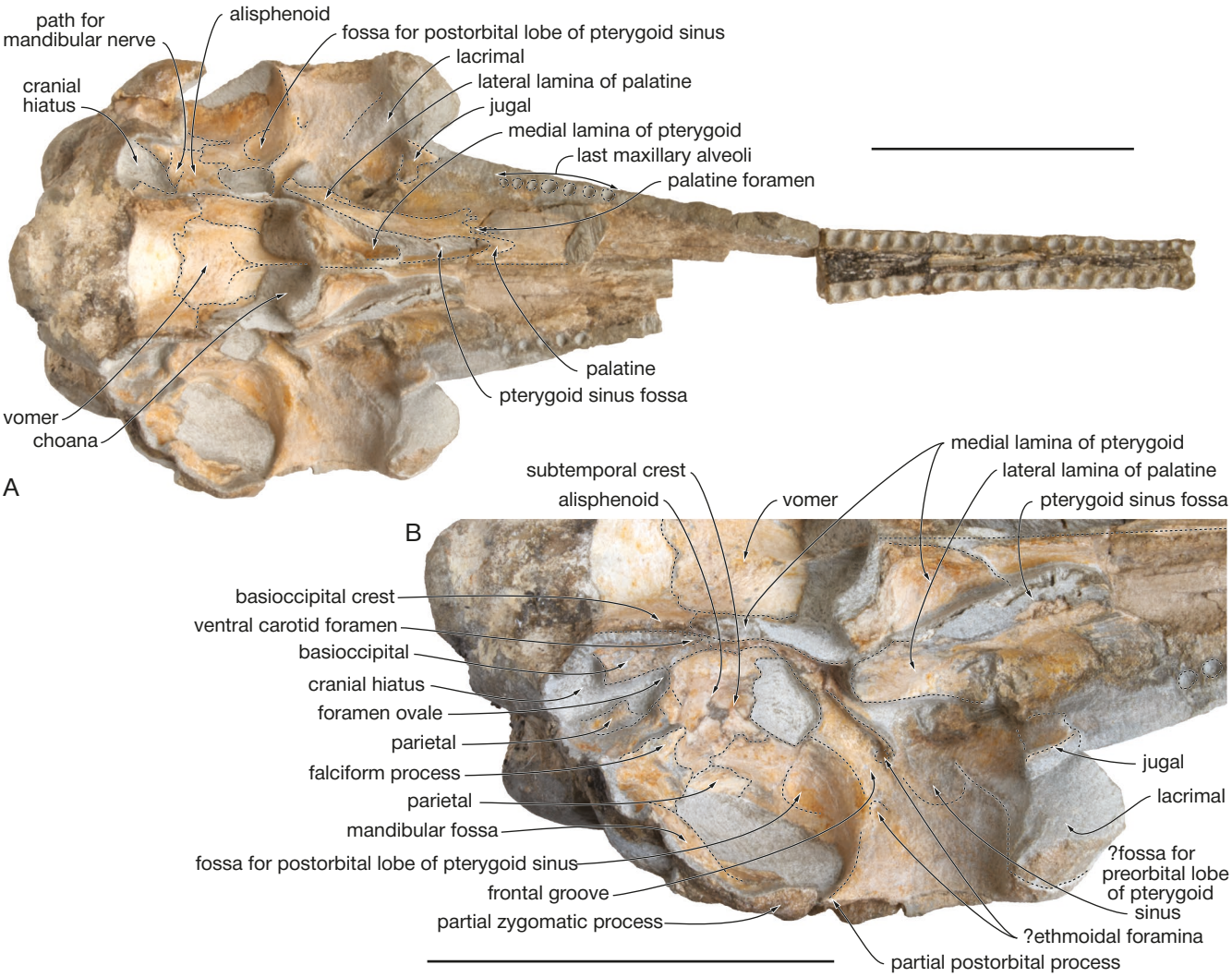

Fig. 7. — Cranium of *Mesokentriodon protohumboldti* n. gen., n. sp. MNHN.F.PPI283 (paratype) in ventral view (**A**) and detail of left side of basicranium and palate in anteroventral and slightly lateral view (**B**). **Dashed lines** for main sutures, bone edges, and other anatomical features. Scale bars: 100 mm. Photos: Olivier Lambert.

surface of the maxilla in the antorbital region is only slightly more elevated than the medial portion of this bone, a feature that is more developed in the paratype. Better defined in the latter specimen, two low and thin maxillary crests, run parallel 9-10 mm from each other, in a posterolateral direction, from this poorly elevated region. Their course is more difficult to follow in the area dorsal to the temporal fossa, but they can be distinguished along the anterior flank of the nuchal crest, likely corresponding to separate origin areas for the facial muscles (possibly, the pars anteroexternus and pars anterointernus, see Heyning 1989). No dorsal exposure of the maxilla medial to the premaxilla could be detected along the bony nares and/or the posterior part of the mesorostral groove.

Along the vertex, the medial edge of the maxilla is abruptly elevated dorsally and dorsolaterally, reaching roughly the same dorsal level as the nasal, and markedly overhanging the more ventral part of the maxilla, providing thus this region with a pinched aspect in posterodorsal view. This edge of the maxilla is anteroposteriorly longer in the paratype (29.5 mm on the left side vs 26 mm on the holotype), corresponding to a longer vertex compared to the holotype. The posterior edge of the maxilla is damaged in both the holotype and paratype, but the preserved parts indicate a narrow exposure of the frontal between the maxilla and the interparietal or parietal on the anterior flank of the nuchal crest. Each maxilla reaches a level that is distinctly posterior to the anteromedial part of the nuchal crest, giving a deeply sigmoidal outline to the anterodorsal margin of the occipital shield in dorsal view.

All the 37 alveoli for maxillary teeth counted on each side of the holotype correspond to single-rooted teeth (Fig. 6). The transverse diameter of the anterior alveoli ranges from 4.5 to 5 mm in the paratype and from 6 to 6.5 mm in the holotype. The corresponding interalveolar septa are high, well-defined, and 1 to 2 mm long. In the better-preserved holotype, the alveoli from the mid-part of the rostrum have a transverse diameter of 6.5 to 7 mm (slightly smaller in the paratype), with generally longer (1.5 to 3 mm) septa in the holotype (contra 1 to 1.5 mm-long septa in the paratype;

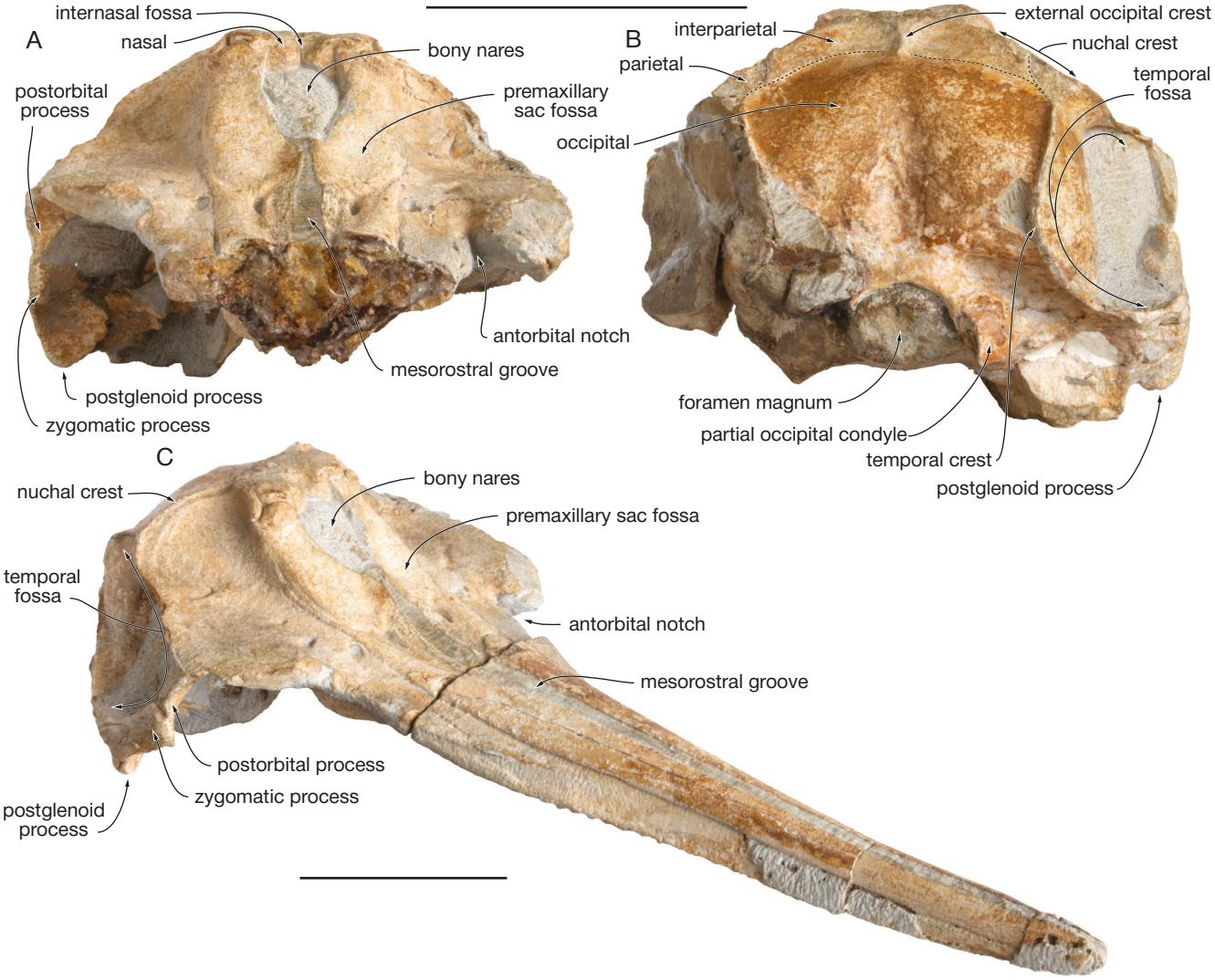

FIG. 8. — Cranium of *Mesokentriodon protohumboldti* n. gen., n. sp. MNHN.F.PPI282 (holotype) in anterior (**A**, lacking most of the rostrum), posterior (**B**), and right anterodorsolateral (**C**) views. **Dashed lines** for sutures. Scale bars: 100 mm. Photos: Olivier Lambert.

Fig. 7). The diameter of the alveoli decreases posteriorly, with the last alveoli having a diameter of 4.5 to 5 mm in the holotype. The last five alveoli gradually detach from the lateral margin of the rostrum. Only partly visible in the holotype, the vomerine trough is deep and narrow along the median third of the rostrum length. The maxilla-premaxilla sutures are visible along the flanks of the trough, diverging anterolaterally and reaching the medial margin of the alveolar row. Only a few palatine foramina are visible: a small one, 1.5 mm in diameter, is found 23 mm anterior to the tip of the right palatine of the holotype, and at least another is found along the palatine-maxilla suture on both sides of the same specimen. The ventral surface of the maxilla is transversely concave in the area between the posterior tract of the alveolar series and the palatine. This depressed area may indicate the presence of an anterior sinus, though the outline of such a depression at the rostrum base does not always correspond to the outline of the anterior sinus in extant delphinidans (see Fraser & Purves 1960).

Palatine

In both the holotype and paratype, the anterior tip of the palatine reaches a level anterior to the last posterior maxillary alveolus (Figs 6-7). The tips of the right and left palatines are distant from each other, the maxilla-palatine sutures drawing a W-shaped outline. From this tip, the suture runs posterolaterally for a short distance, before turning anterolaterally, making a secondary anterior projection before running posteriorly and posteromedially. The constriction of the palatine resulting from this posteromedial direction of the suture is maximal at the level of the antorbital notch. From there, the suture leaves posterolaterally towards the medial edge of the ventral infraorbital foramen. This region features a large and deep depression that marks the dorsalmost portion of the outer surface of the lateral lamina of the palatine. We interpret this depression as part of the site of origin for the pterygoideus internus muscle, based on topological similarities with extant delphinids (Seagars 1982). The narrow anterior part of the pterygoid sinus fossa extends in the palatine until a level just posterior to the last maxillary

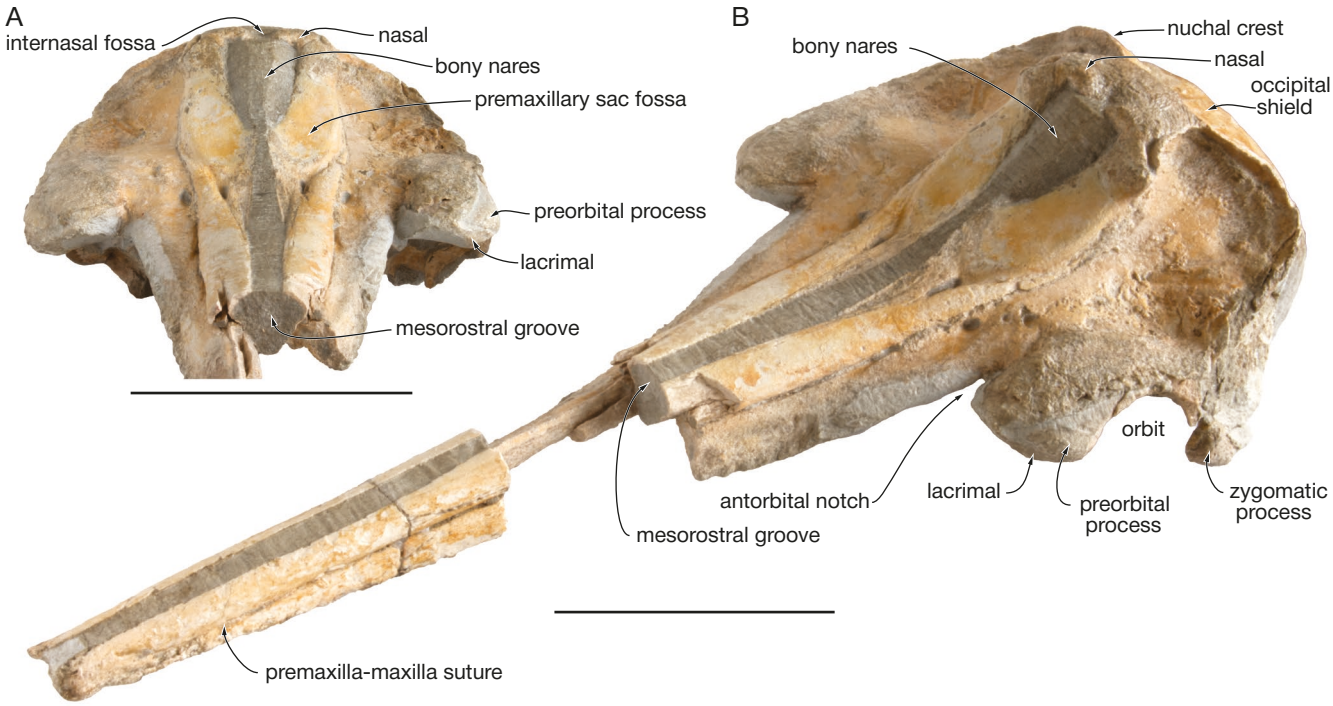

FIG. 9. — Cranium of *Mesokentriodon protohumboldti* n. gen., n. sp. MNHN.F.PPI283 (paratype) in anterodorsal (**A**, lacking part of the rostrum) and left anterodorsolateral (**B**) views. Scale bars: 100 mm. Photos: Olivier Lambert.

alveolus, thus well anterior to the level of the antorbital notch, in the three specimens. The lateral lamina of the palatine is high (35 mm from the medial edge of the ventral infraorbital foramen to the ventromedial edge of the lamina) and extends posterolaterally until the level of the anterior edge of the frontal groove, posterior to mid-orbit length.

Pterygoid

The whole hamular region of the pterygoid is lost in both the holotype and the paratype, but a section in the pterygoid just anterior to the choana in the paratype indicates that at least the posteromedial base of the hamular process was relatively robust (Fig. 7). Similarly, no trace of the lateral lamina of the pterygoid could be found. This bone is preserved along the medial wall of the pterygoid sinus fossa, only covering the palatine for less than half the distance between the choana and the anterior apex of the pterygoid sinus fossa. Better preserved on the paratype, the medial lamina of the pterygoid extends as a thin plate for at least half the length of the basioccipital basin. In this region, the base of the lateral surface of the medial lamina is excavated by a shallow fossa, starting 10 mm anterior to the ventral carotid foramen, which likely corresponds to an extension of the peribullary/pterygoid sinus fossae.

Jugal

The base of the slender styliform process of the jugal is posteromedial to the antorbital notch (Figs 6-7). The sutures with both the maxilla (anteromedially) and the lacrimal (posteriorly) can be distinguished at least locally. The jugal is thus not fully fused with the lacrimal, though the lateral portion of their contact is hidden by sediment.

Lacrimal

In lateral view the lacrimal underlies the preorbital process of the frontal as a thick (up to 7.5 mm) oblique plate that contributes to the robust and ventrally rounded outline of this region, a feature that is visible in the three specimens (Figs 4, 5, 10B). In ventral view, the lacrimal-maxilla suture is directed posteromedially towards the posterior edge of the antorbital fossa, where its outline is more difficult to follow. The lateral margin of the ventral infraorbital foramen is interpreted as being made by the lacrimal. The ventral surface of the lacrimal makes more than one third of the total ventral surface of the orbit. Posterolateral to the base of the styliform process, this surface is depressed, forming a distinct lacrimo-maxillary fossa.

Nasal

The nasals are much transversely wider than the bony nares and slightly wider than the exposure of frontals on the vertex in the holotype, paratype, and MUSM4693; they occupy a dorsal surface greater than that of the frontals (Figs 2-3, 10A). Due to a shorter exposure of the frontals in the holotype compared to the paratype, the nasals reach posteriorly a level closer (5.5 mm) to the occipital shield in the former specimen. The highest point of the nasals is only slightly higher than the frontals. A well-defined internasal fossa that slopes anteroventrally excavates the medial third of both nasals (Figs 2-3, 8A, 9A). This internasal fossa is deeper in the holotype. The high anterior margin of each nasal is cut by a deep vertical notch, which defines an anterolateral spine of the nasal extending anteriorly along the medial edge of the ascending process of the premaxilla. The spine is longer on the holotype, with a tip at least 9 mm anterior to the anteriorly

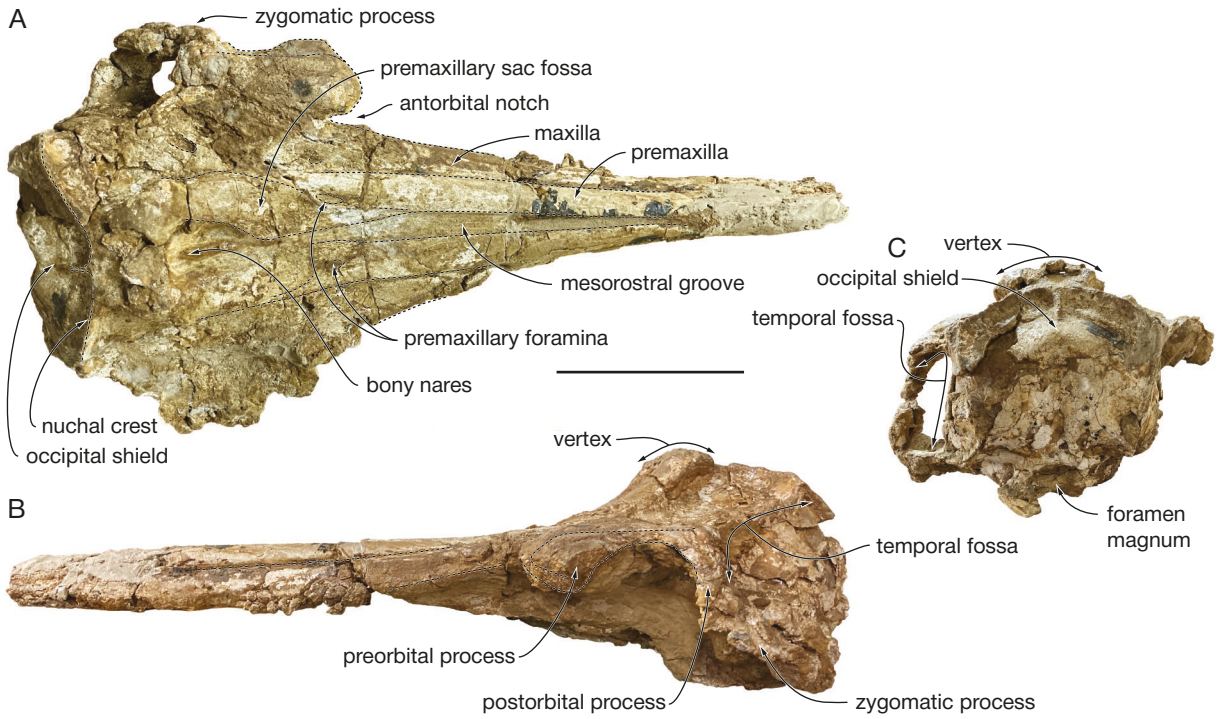

FIG. 10. — Cranium of *Mesokentriodon protohumboldti* n. gen., n. sp. MUSM4693 in dorsal (**A**), left lateral (**B**), and posterior (**C**) views. Scale bar: 100 mm. Photos: Olivier Lambert.

convex anteromedial edge of the nasal. The dorsal surface of the spine is roughly flat, and slopes anteroventrally and slightly medially. Best seen in the holotype, the joined nasal-frontal sutures display a complex, interdigitated outline, drawing a widely open V that points forwards in their medial portion, while the lateralmost part of the suture is roughly laterally directed. In the paratype, the joined sutures display a more regularly convex outline in their medial part.

Frontal

On the vertex, the exposed dorsal surface of the frontals is transversely convex and irregular, marked by numerous thin grooves and crests (Figs 2-3). Anteroposteriorly shorter in the holotype, the frontals are separated in the latter specimen by a deep and narrow (4 mm wide) fossa for most of their medial margin. Such a fossa, which is absent in the paratype, may testify to a subsequently lost separate center of ossification, possibly corresponding to a vestigial anterior median interparietal (Roston *et al.* 2023), an interpretation that should be tested with a CT scan across the vertex region. The internasal fossa does not invade the frontals. The posterior margin of the frontals on the vertex, along the nuchal crest, is slightly anteriorly convex (more distinctly so in the holotype).

Best preserved on the paratype, the robust preorbital process is triangular in lateral view, with a swollen lateral surface that is also seen in MUSM4693 (Figs 4-5, 10B). Its ventral extent (17 mm on the left side of the paratype) reaches not far from the dorsoventral level of the tip of the postorbital process, giving to the dorsal outline of the highly arched orbit a semi-elliptical shape. Only complete on the right side of the holotype, the postorbital process is long (31 mm), slender (with an anteroposterior thickness of 4.5 mm at 6 mm from the tip), and subvertical, only displaying a slight anteroventral curve of the apical portion. The tip of this process is at a close distance (no more than 2 mm) from the anterodorsal margin of the zygomatic process of the squamosal. None of these two parts display any indication (e.g., a fossa or a crest) for a contact, and the condition observed in the holotype is thought to represent the original relationship between the frontal and the squamosal, given the similar position and direction of the nearly complete postorbital process on the left side of the paratype and the lack of any clue for deformation in this area (consider the regular outline of the temporal fossa and of the occipital shield in the holotype). In ventral view, the infratemporal crest is well defined, and somewhat more acute in its medial portion in the holotype (Figs 6-7). Observed in both specimens, the fossa for the postorbital lobe of the pterygoid sinus is anteroposteriorly broader in the paratype, in which it probably partly crossed through the infratemporal crest. A shallower fossa with poorly defined edges is detected between the frontal groove and the antorbital fossa, only shortly invading the lacrimal; it is tentatively interpreted as the fossa for the preorbital lobe of the pterygoid sinus. Anterior to the infratemporal crest, the ventral surface of the frontal groove is pierced by several tiny foramina, some of which may correspond to ethmoidal foramina (or, for the more lateral, to foramina for the frontal diploic vein); on the right side of the holotype, four foramina are detected between the infratemporal crest and the thin oblique plate of the orbitosphenoid that makes the anteromedial margin of the frontal groove. The posteriorly pointed, transversely concave ventral surface of the roof of the temporal fossa is

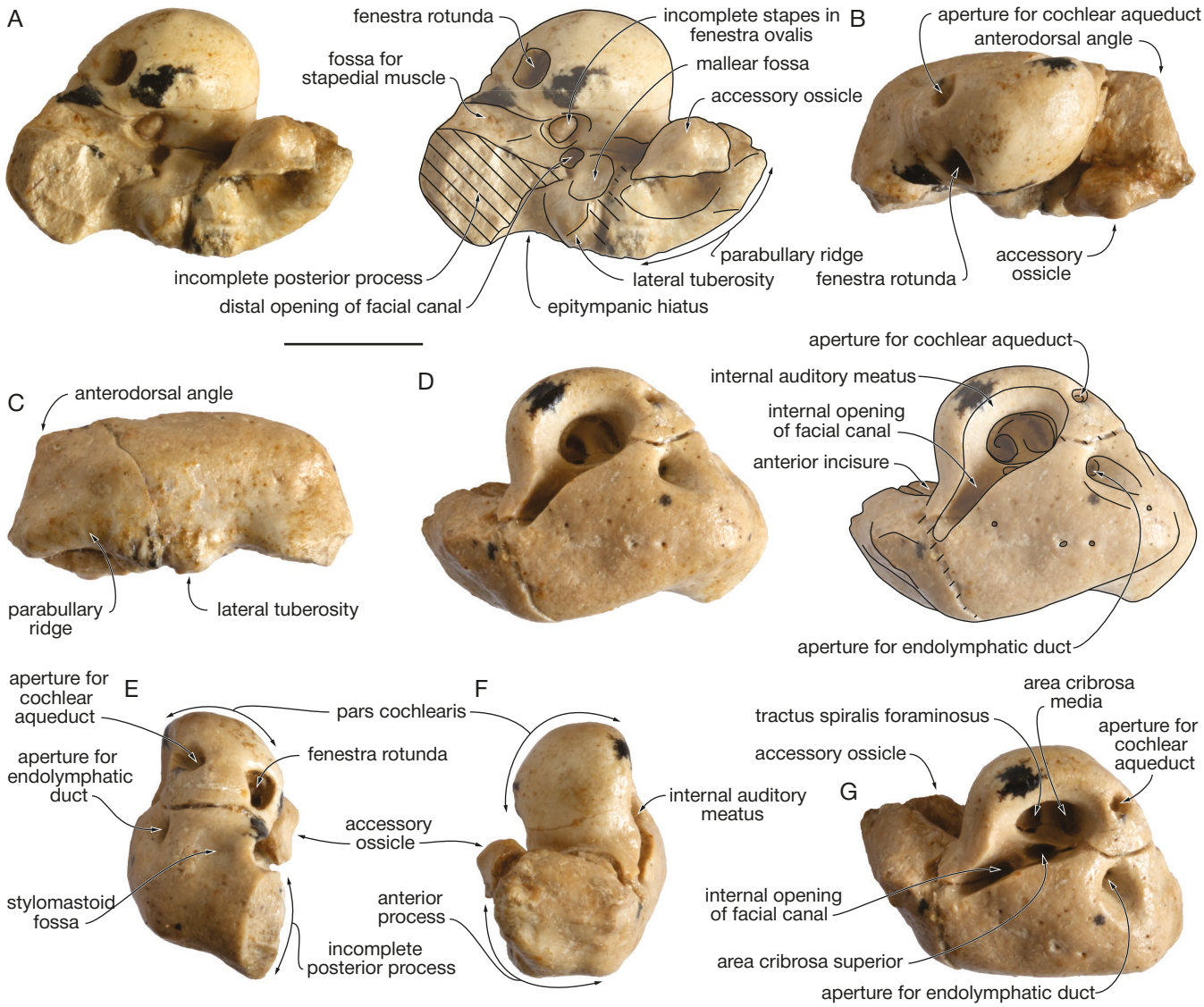

FIG. 11. — Left periotic of *Mesokentriodon protohumboldti* n. gen., n. sp. MUSM4693 in ventral (**A**, with explanatory line drawing), medial (**B**), lateral (**C**), dorsal (**D**, with explanatory line drawing), posterior (**E**), anterior (**F**), and dorsomedial (**G**) views. **Hatching** for break surfaces. Scale bar: 10 mm. Photos: Olivier Lambert.

made by the frontal alone, the interdigitated frontal-parietal suture following the dorsomedial corner of the temporal fossa in a posterolateral direction. Best seen on the right side of the paratype, this suture reaches the highest point of the temporal fossa before turning dorsally along the nuchal crest (Fig. 5A).

Vomer

Due to the presence of indurated sediment in the mesorostral groove and part of the vomerine trough in both the holotype and paratype, as well as to the damaged state of the basicranium in the former specimen, the vomer is only visible in the basioccipital basin of the latter, extending posteriorly for the same distance as the medial lamina of the pterygoid (Fig. 7).

Parietal and interparietal

Combining the right side of the paratype for the frontal-parietal suture and the right side of the holotype for the squamosal-parietal suture, the parietal makes most of the medial wall of the temporal fossa (Figs 4; 5A). This surface is anteroposteriorly and, to a lesser degree, dorsoventrally convex. In ventral view, a narrow stripe of parietal is visible posterior to the alisphenoid and medial to the squamosal on the basicranium of the holotype, being partly covered by sediment (Fig. 6). On the better-preserved occipital shield of the holotype, the parietals may contribute to the dorsolateral portions of the shield as small triangular exposures (longest side of each triangle approximately 15 mm long) (Figs 2; 8B). Medial to this triangle, a dorsal stripe of the shield displays an irregular surface that contrasts with the smooth surface more posteroventrally. The limit between the irregular and smooth surfaces is marked by a small step, with an outline that is reminiscent of the interparietal-occipital suture identified for example in *Tursiops truncatus* (Mead & Fordyce, 2009, fig. 5). This dorsal region with thicker bone is thus interpreted here as being formed by the interparietal. A roughly similar separation is locally found on the right side of the paratype (Fig. 3). In the

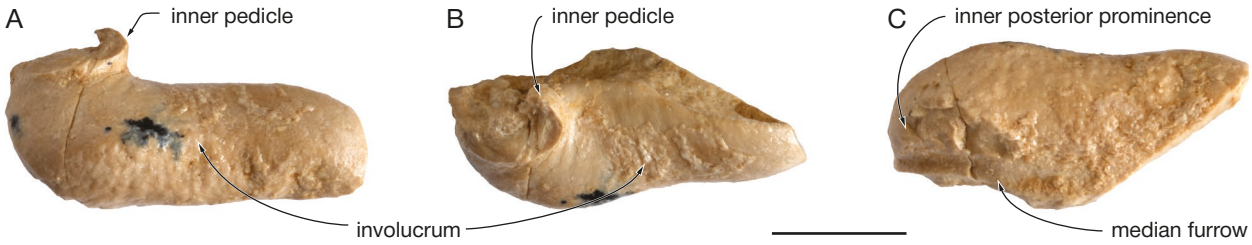

FIG. 12. — Partial left tympanic bulla of *Mesokentriodon protohumboldti* n. gen., n. sp. MUSM4693 in medial (**A**), dorsal (**B**), and ventral (**C**) view. Scale bar: 10 mm. Photos: Olivier Lambert.

holotype, medial to the proposed suture between the parietal and interparietal, the corner of the interparietal bears a small prominence, most likely for neck muscle attachment. Medially, the interparietal of the holotype and MUSM4693 is marked by a thin but prominent external occipital crest, starting on the nuchal crest and extending posteroventrally for a short distance on the occipital (Figs 2, 8B, 10C). Though lower, a similar crest is present on the paratype. Lateral to the crest, the occipital shield is transversely and anteroposteriorly concave.

Supraoccipital

Just posteroventral to the external occipital crest, the occipital shield becomes markedly convex transversely and anteroposteriorly in all specimens. Further posteroventrally, a longitudinal groove broadens and deepens down to a short distance to the foramen magnum, separating two posteriorly bulging areas (Figs 2; 3; 8B; 10C). The right and left temporal crests converge slightly ventromedially until a level 20 mm above the foramen magnum, thus providing the occipital shield with a pinched aspect in posterior view.

Orbitosphenoid and alisphenoid

In both the holotype and paratype, a single large oval opening occurs posteromedial to the frontal groove (Figs 6-7); it does not allow for distinguishing between the optic foramen, the inferior and superior orbital fissures, and the foramen rotundum. As the edges of this confluent opening are all very thin, the differences between the holotype and paratype with respect to its outline (e.g., the opening is more extended anterolaterally in the paratype) are most likely not meaningful. Though the frontal-orbitosphenoid suture is difficult to follow in this region, the latter bone is at least partly preserved in both specimens as a thin, oblique plate making the anteromedial wall of the frontal groove and extending posteromedially along the anterior edge of the large confluent opening. The frontal-alisphenoid suture is easier to follow, zig-zagging posterodorsally for a short distance on the medial wall of the temporal fossa up to the frontal-parietal suture. The alisphenoid extends farther anterodorsally in the holotype, reaching the posteromedial margin of the fossa for the postorbital lobe of the pterygoid sinus. The alisphenoid is exposed as a narrow stripe in the temporal fossa, and this part of the bone is separated from its basicranium part by a thin anterior extension of the subtemporal crest (Fig. 7B). Medioventral to this crest, the ventrolaterally facing surface of the alisphenoid is irregularly concave. Along the posterior margin of the alisphenoid, the large foramen ovale (6 mm of diameter in the paratype) appears to be confluent with the cranial hiatus (see below). The path for the mandibular nerve is broad and well-defined for about 10 mm, passing laterally dorsal to the tip of the falciform process.

Squamosal

The best-preserved squamosal is the right one of the holotype (Fig. 4). The relatively robust (for an early delphinidan) and moderately elongated zygomatic process is directed anterodorsally. In lateral view, the dorsoventrally high (21 mm) anterior margin of this process is subvertical. It draws an angle of about 90 degrees with the ventral margin, making an angular anteroventral corner, while the anterodorsal corner is more rounded. The maximum transverse width of this part of the zygomatic process is 26 mm, taken dorsally. The transversely broad dorsal margin of the process is approximately rectilinear in lateral view, being followed posteriorly by a slight elevation of the supramastoid crest. The thinner ventral margin of the zygomatic process is also roughly rectilinear. It bears an 8 mm-long anteroventral prominence that corresponds to the contact surface with the styliform process of the jugal. The lateral surface of the zygomatic process is covered by small tubercles, as observed in several inioids (e.g., the extinct *Brujadelphis ankylorostris* and the extant *Inia* spp.; Lambert *et al.* 2017). The postglenoid process is robust, with an anteroposterior length of 11 mm and a mediolateral width of 10.5 mm. Its apex reaches a level more ventral than the posttympanic process, but dorsal to the apex of the paroccipital process. In posterolateral view, the posttympanic process is broad, the external auditory meatus being 18 mm distant from the exoccipital. The subcircular sternocephalicus fossa is deep but does not extend anteriorly past the level of the external auditory meatus, thus facing posterolaterally. Though its anterior part remains filled by sediment, the squamosal fossa — making the floor of the temporal fossa (not to be confused with the squamosal fossa on the periotic of some mysticetes; Mead & Fordyce 2009) — is transversely broad (more than 26 mm) and deep, with a marked anteroventral slope of its surface. Like the rest of the medial wall of the temporal fossa, the squamosal plate is anteroposteriorly convex. In this region, the parietal-squamosal suture rises for 28 mm dorsal to the level of the supramastoid crest.

In ventral view, the mandibular fossa is transversely wide (26 mm), and it faces anteriorly and slightly ventrally

(Fig. 6). The tympanosquamosal recess is vast, extending dorsal to the medial edge of the mandibular fossa, deeply excavating the medial surface of the postglenoid process, where it extends nearly as far as the ventral apex of the latter (also seen in MUSM4693). The recess reaches the ventromedial surface of the zygomatic process anterior to the mandibular fossa, at least 9 mm anterior to the level of the anterior edge of the squamosal fossa. In its main medial region, the floor of the recess is irregular, being covered with small, deeper fossae. The plate-like falciform process bears a pointed, narrow anteroventromedial projection with a length of 12.5 mm (taken from the anteromedial margin of the tympanosquamosal recess) in the holotype. Together with the shape of the lateral lamina of the palatine (see above), this condition of the falciform process suggests that, like in most other delphinidans (e.g. Muizon, 1988b), there was no contact between the lateral lamina of the pterygoid (that would be lost in these two specimens) and the squamosal at this level. On the narrow external auditory meatus (2 mm wide at mid-length in the holotype), the anterior meatal crest appears to be higher than the posterior meatal crest, though this region is not optimally prepared. The spiny process is interpreted as ending 27 mm medial to the outer opening of the meatus.

Exoccipital

Only the upper part of the right occipital condyle is preserved in the holotype (Figs 4, 8B), showing a moderately well-defined (i.e. short but distinct) neck. Based on the natural endocast, the foramen magnum should have been wider (more than 33 mm) than high (26 mm), oval in outline, and with an only slight dorsomedial elevation (i.e. no distinct opisthion). The dorsal condyloid fossa is very deep, extending up to 10 mm anterior to the anterolateral edge of the condyle. Only partly preserved on the right side of the holotype, the more lateral part of the exoccipital is directed anterolaterally, being overhung by the temporal/supramastoid crest. Also incomplete, the ventral margin of the exoccipital was originally anterior to the level of the occipital condyle and reached more ventrally than the postglenoid process.

Basioccipital and basisphenoid

Only the anterodorsal portions of the basioccipital crests are preserved in the paratype (Fig. 7). Their section is transversely thin. The left and right crests are 51 mm distant from each other anteriorly. The jugular notch is partly preserved on the right side of the holotype; its anterior section is broad and U-shaped. Dorsolateral to the basioccipital crest, the basioccipital contributes to the partial closure of the space in between the foramen ovale and the cranial hiatus (best seen on the left side of the paratype). With a transverse diameter of 2 mm, the ventral carotid foramen is 10 mm anteromedial to the foramen ovale along the lateral surface of the basioccipital crest, just posteromedial to the oblique suture between the medial lamina of the pterygoid and the basisphenoid.

Periotic

The left periotic of MUSM4693 is well preserved, only missing most of the posterior bullar facet and the distalmost part of the posterior process and displaying a couple of fractures across the whole bone with minimum to no displacement and some slight damage to the anterior portion of the lateral tuberosity (Fig. 11). The accessory ossicle of the tympanic is preserved attached in the fovea epitubaria and the partial stapes is held in situ in the fenestra ovalis (see below). The periotic has a length of more than 24.8 mm (see all dimensions in Table 1). Based on the dorsal outline of the posterior process in lateral view, the size of the break cross section, and the general shape similarities with the periotic of *Kentriodon pernix* USNM 8060 (Kellogg 1927, plate 3), the total length probably did not exceed 25.3 mm.

The anterior process is shorter than the pars cochlearis. At mid-length, it is slightly dorsoventrally thicker than mediolaterally wide (not taking into account the accessory ossicle). In ventral view (Fig. 11A), it turns regularly anteromedially, with slightly convex medial wall of the parabullary ridge. The anteroventral tip of the anterior process bears a few small tubercles that make its outline locally somewhat more robust. In medial view (Fig. 11B), the anterodorsal angle is prominent, with an angle of 120° between the rectilinear dorsal and anterior margins. The anterodorsal angle is posterior to the level of the anteroventral tip of the process. Best seen in dorsal view (Fig. 11D), as it is partly hidden by the accessory ossicle in ventral view, the anterior incisure is broad and U-shaped, the medial surface of the anterior process being well removed from the anterior surface of the pars cochlearis. In lateral view (Fig. 11C), the surface of the anterior process is slightly depressed just dorsal to the recurved parabullary ridge.

The pars cochlearis is proportionally high in the medial direction and moderately tilted anteriorly in ventral view. Its anteromedial margin is more angular than its posteromedial margin. The ventral and medial surfaces of the pars cochlearis are regularly convex, with no trace of a median promontorial groove. In medial view, the pars cochlearis has a nearly flat dorsal outline, corresponding to the medial edge of the internal auditory meatus (IAM), and its long axis in this view is oblique, directed anteriorly and slightly anterodorsally. The maximum ventral bulging is located anterior to the fenestra rotunda. The latter is large, with a diameter of 2.8 mm and a semi-circular outline. Its mediodorsal corner is followed mediodorsally by a shallow, short sulcus. The aperture for the cochlear aqueduct is small and roughly circular (diameter 1.5 mm), opening dorsomedioposteriorly at a short distance (1 mm) from the IAM. More distant from the IAM (2.8 mm), the aperture for the endolymphatic duct has similar dimensions (maximum diameter 1.4 mm), is slightly dorsoventrally flattened and opens posterolaterodorsally, being followed by a broad groove for 3 mm towards the posterodorsal corner of the periotic (= dorsal tuberosity in Mead & Fordyce 2009). The IAM is vast, occupying a large part of the dorsal surface of the pars cochlearis, and tear-shaped, extending as a deep, U-shaped sulcus up to the anterolateral limit of the pars cochlearis (Fig. 11D, G). The anteromedial edge of the IAM

is more rounded in section than the acute posterolateral edge. The tractus spiralis foraminosus and the area cribrosa media (see Orliac *et al.* 2020 for terminology, as well as Ichishima *et al.* 2021 for an alternative set of anatomical terms) are separated from the laterally located area cribrosa superior (singular foramen in Mead & Fordyce 2009) by a thin crista transversa (or transverse crest). The latter is much narrower, but similar in height to the perpendicular crest, which separates the area cribrosa superior from the anterolaterally located internal opening of the facial canal. The top surface of the broad (about 1 mm wide) perpendicular crest is excavated by a shallow fossa. The internal opening of the facial canal is more anterior than the tractus spiralis foraminosus, but does not reach the anterolateral corner of the pars cochlearis, which is excavated by the U-shaped sulcus that leaves from this opening. Posterolateral to the IAM, the superior process is barely developed, only projecting 1.5 mm dorsal to the level of the medial margin of the IAM and displaying a nearly flat (only slightly convex) dorsal outline in medial view, without any distinct crest.

The fenestra ovalis (with the in situ partial stapes) has an oval outline, with an anteromedially directed long axis (Fig. 11A). Posterior to the fenestra ovalis, the lateral caudal tympanic process (sensu Lambert *et al.* 2018) is barely defined; the medial edge of the fossa for the stapedial muscle undulates slightly, without any distinct lateral projection. The fossa for the stapedial muscle is broad (2.6 mm) and extends posteriorly to the incomplete posteromedial margin of the posterior process, being separated from the facial sulcus by a low, thin oblique ridge. From this ridge, the short facial sulcus turns anterolaterally and then anteriorly to the distal opening of the facial canal. The latter is anterior to the level of the fenestra ovalis. Dorsal to the posterior end of the fossa for the stapedial muscle, the posteromedial surface of the posterior process is excavated by a shallow but well-defined stylomastoid fossa, with a dorsoventral diameter of about 3 mm. In medial view, the dorsal margin of the posterior process turns abruptly posteroventrally, indicating a short main part of the posterior process. The posterior break surface of this process (Fig. 11E) suggests that the dorsoventrally thin posterior tip of the process and the posterior bullar facet should have turned posteroventrally to some extent, as e.g. in *Kentriodon pernix* USNM 8060. The lateral tuberosity is anteroposteriorly long (8 mm) but projects only little laterally. Consequently, the epitympanic hiatus is shallow (at least with respect to its anterior wall, as the posterior wall is incomplete, due to the missing posterior bullar facet). The broad (mediolateral diameter 3.1 mm) and shallow mallear fossa faces ventrally and slightly medially. The fossa incudis could not be detected, but is thought to have been lost together with the posterior bullar facet.

Tympanic bulla

Preserved in situ within the fovea epitubaria of the periotic, the detached left accessory ossicle is 7.3 mm long anteroposteriorly and 4.3 mm wide mediolaterally (Fig. 11A). Anteriorly, it reaches a level 2.6 mm posterior to the anteroventral tip of the anterior process of the periotic.

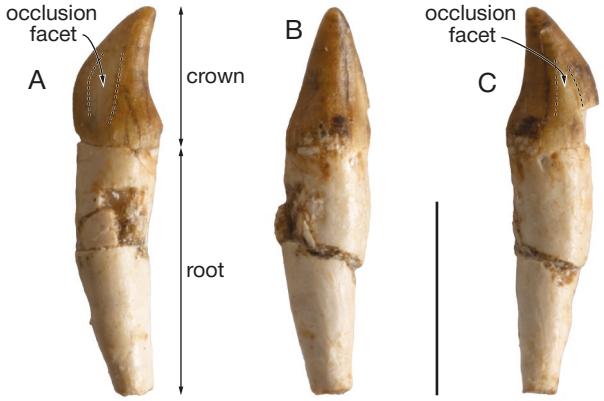

Fig. 13. — Detached posterior lower right tooth of *Mesokentriodon protohumboldti* n. gen., n. sp. MUSM4693 in mesial (**A**), lingual (**B**), and distal (**C**) view. Scale bar: 10 mm. Photos: Olivier Lambert.

The main preserved part of the left tympanic (preserved length = 27 mm) is the involucrum, which only lacks its anterior tip (Fig. 12). At about mid-length of the bone, the involucrum is 9.5 mm thick dorsoventrally. Its dorsal and ventral margins are subparallel for most of its length, except for a moderate anteroventral slope of the dorsal margin in the anteriormost 5 mm. The inner posterior prominence has a regularly rounded outline in medial view, with no distinct corner. In dorsal view, the medial margin of the tympanic is convex along its posterior half, transitioning anteriorly to a slightly concave region that is further followed by the convex anteriormost part. The maximum mediolateral width of the involucrum (10.6 mm) is found in its posterior region, just anterior to the partly preserved inner pedicle. From that level, the lateral margin of the involucrum gradually turns anteromedially, with a thickness decreasing down to 5 mm at the preserved anterior tip. In ventral view, the inner posterior prominence is narrow (5-6 mm) and laterally margined by a deep median furrow (Fig. 12C). Only partly preserved, the latter extends for at least two thirds of the preserved length of the tympanic.

Stapes

The basal part of the stapes, which is kept in situ in the fenestra ovalis, has an oval outline (the long axis is 2.3 mm long) (Fig. 11A). It is proposed that the stapes broke across the anterior crus, possibly at the level of a vestigial stapedial foramen.

Teeth

One subcomplete detached tooth of MUSM4693, interpreted as a posterior lower right tooth based on the crown-to-root proportion, crown curvature, and root curvature (see below), has been prepared and is described here (Fig. 13). Only missing the tip of the root, it is 19.6 mm long, including a 7.8 mm-long crown. Labiolingual and mesiodistal diameters at the crown base are 4.3 and >4.0 mm, respectively. The crown is curved apicolingually, with a slight bulge on the lingual surface, just above the root-crown boundary. The thin (0.2 mm, measured along a minor break surface) enamel layer

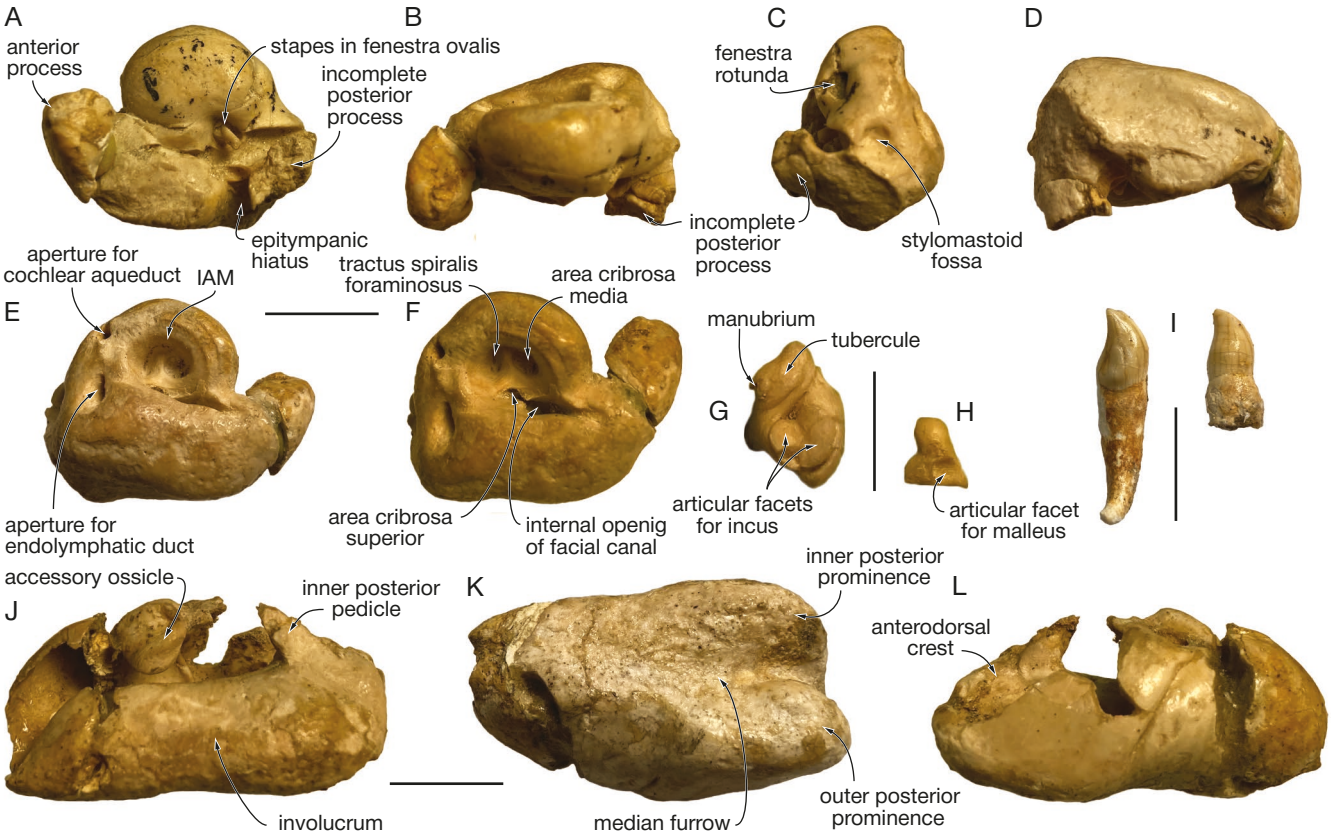

FIG. 14. — Periotic, malleus, incus, tympanic bulla, and teeth of *Incacetus broggii* AMNH32656 (holotype): right periotic in ventral (**A**), medial (**B**), posterior (**C**), lateral (**D**), dorsal (**E**), and dorsomedial (**F**) views; right malleus in posteromedial view (**G**); right incus in medial view (**H**); two detached posterior teeth in mesial or distal view (**I**); right tympanic in medial (**J**), ventral (**K**), and lateral (**L**) views. Scale bars: A-F, I-L, 10 mm; G, H, 5 mm. Photos: Olivier Lambert.

is consistently smooth. The root is roughly rectilinear. While no apical wear facet could be detected, shallow wear surfaces along the distal and mesiolabial surfaces of the crown likely witness the occlusion with the preceding and succeeding upper teeth. The pulp cavity is nearly completely filled, with only a tiny (0.1 mm) opening observed at the center of the cross section of the tip of the root.

Several broken upper teeth are preserved in situ in the region of the left upper alveolar series about 160 mm anterior to the level of the antorbital notch in MUSM4693 (Fig. 10B). Their diameter at the crown base is 4.5 mm.

COMPARISONS

Affinities with early delphinidans generally referred to the family Kentriodontidae are supported by the following combination of characters: lack of contact between premaxilla and frontal on the vertex, retention of a broad contact between premaxilla and nasal, knob-like posterior end of the premaxilla, presence of an internasal fossa and of a vertical notch along the anterior margin of the nasal, absence of an anterior bullar facet on the periotic, and subrectangular outline of the anterior process of the periotic in lateral view (Barnes 1985; Muizon 1988b; Lambert *et al.* 2005; see also Lambert *et al.* 2017; Peredo *et al.* 2018; Kimura & Hasegawa 2019; Guo & Kohno 2023 for the debated phylogenetic relationships and possible non-monophyly of this family).

Within this large group of Miocene dolphins, *Mesokentriodon protohumboldti* n. gen., n. sp. is considerably smaller (using the bizygomatic width and/or the width of the occipital condyles as body size proxies) than *Cammackacetus hazenorum*, *Hadrodelphis calvertensis*, *Kampholophos serrulus*, *Lophocetus calvertensis*, *Macrokentriodon morani*, *Miminiacetus pappus*, *Platysvercus ugonis*, and *Wimahl chinookensis*. The largest species *C. hazenorum*, *H. calvertensis*, *Mi. pappus*, and *Ma. morani* also display higher temporal crests and larger temporal fossae compared to *M. protohumboldti* n. gen., n. sp.

Among the small to medium-size early delphinidans, it differs from *Atocetus* spp., *Leptodelphis stavropolitanus*, *Lophocetus repenningi*, *Pithanodelphis cornutus*, *Sarmatodelphis moldavicus*, and *Sophianaecetus commenticus* in the more limited transverse 'pinching' of the posterior part of the vertex, resulting in the exposure of the frontals on the vertex being broader than the bony nares (also a difference with the larger *H. calvertensis*, *L. calvertensis*, and *Mi. pappus*).

Because the holotype and only known specimen of *Incacetus broggii* AMNH 32656 was discovered in the same region of the East Pisco Basin, and presumably in the same beds of the Pisco Formation (the "Santa Rosa vertebrate level", P0 allomember), as the holotype and paratype of *M. protohumboldti* n. gen., n. sp. (Colbert 1944; Muizon 1988a; Marx *et al.* 2017), a more detailed comparison with this poorly known early delphinidan species is provided here. While the

dimensions of the preserved teeth are similar, the cranium is considerably smaller in *M. protohumboldti* n. gen., n. sp., as demonstrated by the smaller transverse diameter of the mesorostral groove (26 mm at a level 155 mm anterior to nasals in *I. broggii*, contra 20 mm at a level 160 mm anterior to nasals in the paratype of *M. protohumboldti* n. gen., n. sp.), the smaller width of the left bony naris (at least 18 mm in *I. broggii*, measured on the endocast of the naris, contra less than 14.5 mm in *M. protohumboldti* n. gen., n. sp.), the shorter horizontal distance between the bony nares and the occipital condyles (estimated at 114 mm in *I. broggii*, contra 82 mm in MNHN.F.PPI282), and the shorter distance between the posterolateral margins of the basioccipital crests (101 mm in *I. broggii*, contra no more than 82 mm in *M. protohumboldti* n. gen., n. sp.). The periotic of *M. protohumboldti* n. gen., n. sp. MUSM4693 differs from *I. broggii* (Fig. 14) in the anteroposteriorly shorter pars cochlearis, the longer anterior process, and the smaller dorsoventral thickness (Tables 1; 2). Furthermore, the anterior process is less medially and ventrally deflected, the anterodorsal angle on the anterior process is better defined, the superior process is more reduced, the aperture for the cochlear aqueduct is larger, and the epitympanic hiatus is shallower. Finally, on the tympanic the involucrum is dorsoventrally thinner in *M. protohumboldti* n. gen., n. sp. (Figs 11, 14; Tables 1, 2).

Originating from younger levels of the Pisco Formation in Cerro la Bruja (Cerro la Bruja vertebrate level, base of allomember P2 or possibly top of P1, see Di Celma *et al.* 2017), the early delphinidan *Belonodelphis peruanus* displays a nasal that is roughly similar in outline to the nasals of *M. protohumboldti* n. gen., n. sp. (Muizon 1988a). However, the rostrum of *M. protohumboldti* n. gen., n. sp. is considerably shorter, its tooth count is much lower, the dorsal exposure of the maxilla at the rostrum base is broader, the posterior process of the periotic is shorter (best seen in lateral view), the anterodorsal angle on the anterior process is more acute, and the dorsal outline of the periotic is roughly flat instead of distinctly convex.

Mesokentriodon protohumboldti n. gen., n. sp. differs from the late Early Miocene species *Rudicetus squalodontoides* in the higher tooth count, smaller dental alveoli, the premaxillary foramen being located at the level of the antorbital notch, the anteriorly longer pterygoid sinus fossa, the presence of a vertical notch along the anterior margin of the nasal, the nasals being larger compared to the frontals on the vertex, the posterior part of the vertex being wider than the bony nares, and the zygomatic process of the squamosal being shorter.

It differs from the Early to early Middle Miocene species *Brevirostrodelphis dividus* (previously *Delphinodon dividum*) in the longer rostrum, the higher tooth count, the wider dorsal opening of the mesorostral groove along the whole rostrum, the narrower antorbital notch, the anteriorly longer pterygoid sinus fossa, the marked step between the lateral margin of the premaxillary sac fossa and the maxilla, the narrower ascending process of the premaxilla, the dorsally higher vertex, the anteromedially shorter nasals with a deeper internasal fossa, the transversely broader posterior part of the vertex, the anterodorsal angle of the periotic being posterior to the anteroventral tip of the anterior process, the broader anterior incisure, the more reduced superior process, the tear drop-shaped internal auditory meatus, the more medially located aperture for the cochlear aqueduct, and the shallower stylomastoid fossa.

TABLE 2. — Measurements (in mm) of the right periotic, tympanic bulla, malleus, and incus of *Incacetus broggii* AMNH32656 (holotype).

	***Incacetus broggii* AMNH32656**
mediolateral width of periotic	17.6
dorsoventral thickness of periotic	13.1
length of anterior process of periotic	e6.2
length of pars cochlearis (from anterior margin to anterior margin of fenestra rotunda)	11.5
total length of tympanic bulla (without posterior process)	33.8
maximum width of tympanic bulla	17.6
maximum dorsoventral thickness of involucrum	9.8
maximum height of malleus in posteromedial view	6.1
maximum width of malleus in posteromedial view	3.8
maximum heigh of incus	2.9

It differs from the late Middle Miocene species *Tagicetus joneti* in the proportionally shorter rostrum, the higher count of maxillary teeth, the wider dorsal opening of the mesorostral groove along the whole rostrum, the V-shaped antorbital notch, the less anteriorly pointed antorbital region in dorsal view, the rounded ventral outline of the preorbital region in lateral view, the premaxillary foramen being located at the level of the antorbital notch, the broader dorsal exposure of the maxilla at rostrum base, and the convex dorsal surface of the vertex in lateral view.

It differs from the late Middle Miocene species *Westmorelandelphis tacheroni* in the larger alveoli for maxillary teeth, the slightly transversely narrower and dorsally higher vertex, the less dorsally inflated nasals, the more oblique suture between nasal and frontal on the vertex, with the lateral part of each nasal being distinctly anteroposteriorly longer than the medial part, the more sigmoidal outline of the nuchal crest in dorsal view, and the dorsoventrally higher temporal fossa.

It differs from the Middle Miocene species *Herbeinodelphis nancei* in the larger size, the lower tooth count, the more medially curved and more pointed (in lateral view) anterior process of the periotic, the more reduced superior process, and the much less posteriorly extended posterior process of the periotic.

It differs from the Middle Miocene species *Pictodelphis kidwellae* in the larger size, the wider dorsal opening of the mesorostral groove along the whole rostrum, the dorsally lower presphenoid anterior to the bony nares, the dorsoventrally thinner lateral margin of the rostrum at its base, the proportionally broader nasals, the shallower internasal fossa, and the less pointed projection of the frontals in between the nasals on the vertex.

In addition to its smaller size, it differs from the late Early Miocene species *Platysvercus ugonis* in the premaxil-

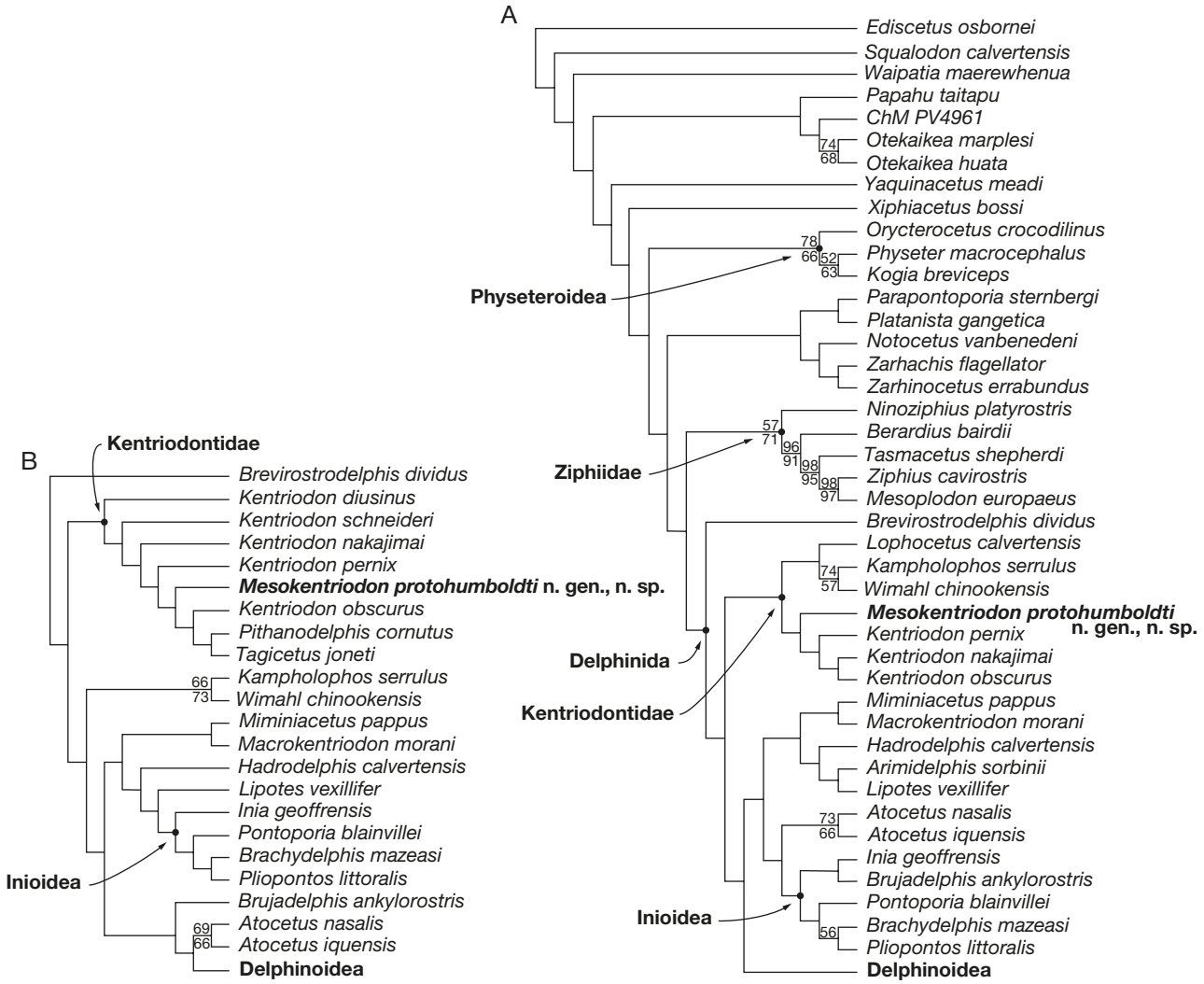

Fig. 15. — Phylogenetic relationships of *Mesokentriodon protohumboldti* n. gen., n. sp. with other early delphinidans: **A**, single most parsimonious tree resulting from the heuristic search based on the morphological matrix with the deletion of 45 taxa for which most of the periotic scores are lacking, with implied weights (K = 3) and with a molecular constraint as a backbone. Tree length = 4294; CI = 0.17; RI = 0.48. Mysticeti and early stem Odontoceti are omitted and Delphinoidea is collapsed for clarity (see complete tree in Appendix 4). The positions of *Arimidelphis sorbinii* (sister group to *Lipotes vexillifer*) and *Parapontoporia sternbergi* (sister group to *Platanista gangetica*) are extremely unlikely, as the former is a delphinid (Bianucci 2005) and the latter a lipotid (Muizon 1988b), as confirmed in many other analyses (including some in Appendix 4). **B**, early delphinidan part of the single most parsimonious tree resulting from the heuristic search based on the morphological matrix with the addition of five 'kentriodontid' s.l. species for which most of the periotic scores are lacking, with implied weights (K = 12) and with a molecular constraint as a backbone (see complete tree in Appendix 4). Tree length = 4353; CI = 0.17; RI = 0.48. Bootstrap and jackknife support values higher than 50 are shown respectively above and below the corresponding nodes.

lary foramen being located at the level of the antorbital notch, the transversely wider vertex, the nasal being higher than the frontal on the vertex, the presence of an internasal fossa, the occipital shield being projected anteromedially, the anteriorly much longer pterygoid sinus fossa, the more slender zygomatic process in lateral view, and the dorsally higher temporal fossa.

In addition to its smaller size, it differs from the Early Miocene species *Wimahl chinookensis* in the higher tooth count, the absence of contact between the premaxillae above the mesorostral groove, the broader antorbital notch, the frontals being longer on the vertex, the proportionally shorter anterior process of the periotic, the anterodorsal angle of the periotic being posterior to the anteroventral tip of the anterior process, and the more voluminous pars cochlearis.

In addition to its smaller size, it differs from the Middle Miocene species *Kampholophos serrulus* in the larger distance between premaxillae above the mesorostral groove in the anterior part of the rostrum, the much lower temporal crests, the dorsally lower temporal fossa not reaching the level of the vertex, the proportionally broader occipital shield, the more anteriorly tilted pars cochlearis with a subvertical anterior margin in ventral view, and the less posteriorly extended posterior process of the periotic.

Among species of *Kentriodon*, *M. protohumboldti* n. gen., n. sp. shares striking similarities with the late Early to Middle Miocene type species *Kentriodon pernix* in terms of the tooth count, morphology of the facial area, vertex, and zygomatic process of the squamosal, giving the impression of an enlarged version of that species. The cranium of

M. protohumboldti n. gen., n. sp. is indeed larger (see Kellogg 1927, p. 22), with a proportionally longer rostrum and larger teeth. It further differs in the more rounded ventral outline of the preorbital region, the more rounded outline of the nasal-frontal sutures on the vertex, and the higher external occipital crest. The periotic is also very similar, only differing in the somewhat dorsoventrally thicker anterior process, more pointed anterodorsal angle, and more reduced superior process.

It differs from the early Middle Miocene *Kentriodon obscurus* LACM 21256 (see comments on the taxonomic status of this species in Nobile *et al.* 2024, where the referral of the cranium LACM 21256 to the same species as the isolated type periotic is questioned) in the larger size, larger alveoli for maxillary teeth, broader antorbital notches, and the higher number of dorsal infraorbital foramina in the antorbital region.

It differs from the Middle Miocene *Kentriodon hobetsu* in the larger size, the anteriorly longer pterygoid sinus fossa, the transversely broader posterior part of the vertex, and the broader anteromedial projection of the occipital shield.

It differs from the poorly preserved holotype cranium of the Early to Middle Miocene *Kentriodon schneideri* in the anteriorly longer pterygoid sinus fossa, the dorsally lower presphenoid anterior to the bony nares, the shorter anteromedial projection of frontals between nasals, the more slender postorbital process of the frontal, a well-defined fossa for the postorbital lobe of the pterygoid sinus, and the more sigmoidal outline of the nuchal crest in dorsal view.

It differs from the late Middle to early Late Miocene '*Kentriodon*' *hoepfneri* (see comments on the systematic affinities of this taxon in Nobile *et al.* 2024) in the roughly vertical postorbital process of the frontal, the anteromedial edge of the nasal being shorter than the anterolateral projection, the less medially projected anterior process of the periotic with a broader anterior incisure, the anterodorsal angle being posterior to the anteroventral tip of the anterior process, the more reduced superior process, and the less posteriorly extended posterior process.

It differs from the Middle Miocene *Kentriodon diusinus* in the larger size, the proportionally longer rostrum, the probably higher tooth count, the premaxillary foramen being located at the level of the antorbital notch, the absence of a contact between premaxilla and frontal on the vertex, each frontal on the vertex not being longer than wide, and the posteriorly much shorter external occipital crest.

It differs from the late Middle to early Late Miocene *Kentriodon nakajimai* in the larger and more closely spaced maxillary alveoli, the premaxillary foramen being located at the level of the antorbital notch, the less defined maxillary crest, the less anteromedially pointed frontals on the vertex, the dorsoventrally thicker anterior process of the periotic with a better-defined anterodorsal angle, the more voluminous pars cochlearis, and the less posteriorly extended posterior process.

It differs from the late Early to early Middle Miocene *Kentriodon sugawarai* in the somewhat smaller size, the dorsoventrally thicker preorbital process, the nasal being higher than the frontal on the vertex, the presence of an internasal fossa, the nasal being distant from the nuchal crest, the rounded anterior outline of the occipital shield in dorsal view, the anteriorly much longer pterygoid sinus fossa, the proportionally shorter anterior process of the periotic, and the more voluminous pars cochlearis.

Finally, the maxillary alveoli are proportionally larger than in all species of *Kentriodon* for which this character is known (see Nobile *et al.* 2024; fig. 9), with a ratio between the alveolar diameter and preorbital width of the cranium ranging between 0.033 and 0.036 in the paratype.

PHYLOGENETIC ANALYSES

As for previous analyses based on an earlier version of this matrix, preliminary tests revealed a high volatility for many odontocete taxa, especially those for which no ear bones could be scored. For a first series of analyses (implied weights with various values of K and equal weights), we deleted 45 taxa for which a majority of codings are missing for the periotic. In some of the analyses (implied weights with K = 3, 12; equal weights), part of the kentriodontids s. l. (including *Mesokentriodon protohumboldti* n. gen., n. sp.) are recovered as stem delphinidans, while in other analyses (K = 6, 9), most 'kentriodontids' s.l. fall in a clade that also includes lipotids and inioids. *M. protohumboldti* n. gen., n. sp. is consistently found in a clade with the three species of *Kentriodon* (*Kentriodon nakajimai*, *Kentriodon obscurus*, and *Kentriodon pernix*) retained for this first round of analyses (K = 3, 6, 9, 12; equal weights), this clade being either sister-group to a clade including *Lophocetus calvertensis*, *Kampholophos serrulus*, and *Wimahl chinookensis* (K = 3, 6, 9), or branching after *Brevirostrodelphis dividus* and before a clade including *Ka. serrulus* and *W. chinookensis* (K = 12; equal weights) (see Fig. 15A for part of the tree with K = 3 and Appendix 4 for all complete trees).

For a second set of analyses, we added five early delphinidan taxa that were originally deleted due to the lack of scores for the periotic, namely, *Kentriodon diusinus*, *Kentriodon schneideri*, *Pithanodelphis cornutus*, *Tagicetus joneti*, and *Rudicetus squalodontoides*. In one of the analyses (K = 12), part of the 'kentriodontids' s.l. (including *M. protohumboldti* n. gen., n. sp.) are recovered as stem delphinidans; in another analysis (K = 6), most 'kentriodontids' s.l. are recovered as stem delphinoids; and in two other analyses (K = 3; equal weights), most 'kentriodontids' s.l. fall in clade that also includes lipotids and inioids. In a last analysis (K = 9), relationships of 'kentriodontids' s.l. are very unlikely, as part of them are recovered as stem odontocetes and others branch after physeteroids and before ziphiids; the results of this analysis are thus not further commented. *M. protohumboldti* n. gen., n. sp. is either (i) sister-group to *K. schneideri* + *K. obscurus*, in a clade that also includes *T. joneti* and *P. cornutus* (K = 3), or (ii) sister-group to *T. joneti* in a clade that also includes *K. pernix*, *K.*, and *K. schneideri* (K = 6), or (iii) sister-group to a clade that includes

K. obscurus, *P. cornutus*, and *T. joneti*, in a larger clade with *K. pernix*, *K. nakjimai*, *K. schneideri*, and *K. diusinus* (K = 12), or (iv) in an unresolved polytomy with *K. pernix*, *K. nakajimai*, *K. schneideri*, and a clade that includes *K. obscurus*, *K. diusinus*, and *R. squalodontoides* (equal weights) (see Fig. 15B for part of the tree with K = 12 and Appendix 4 for all complete trees).

Thus, we could not find a consensus for the phylogenetic relationships of *M. protohumboldti* n. gen., n. sp., and although some analyses reveal closer relationships with some species of *Kentriodon*, others point to affinities with other species outside *Kentriodon* (e.g., *P. cornutus*, *R. squalodontoides*, and *T. joneti*). Nonetheless, our results suggest that *M. protohumboldti* n. gen., n. sp. can be confidently assigned to the family Kentriodontidae as defined above.

The content of the monophyletic family Kentriodontidae varies extensively from one analysis to the other, with seven to 12 species being included depending on the analysis settings (Appendix 4): 11 species comprise this family in the analysis with K = 3, excluding *B. dividus* (stem delphinidan), *Miminiacetus pappus* (lipotid), *Hadrodelphis calvertensis*, *Macrokentriodon morani*, and *Atocetus* spp. (later-branching stem inioids); 12 species in the analysis with K = 6, excluding *M. pappus* and *Ma. morani* (stem delphinidans), *H. calvertensis* (stem to Lipotidae + Inioidea), *P. cornutus* and *Atocetus* spp. (later branching stem delphinoids); eight species in the analysis with K = 12, excluding *B. dividus* (earlier branching stem delphinidan), *Ka. serrulus* and *W. chinookensis* (later-branching stem delphinidans), *Mi. pappus*, *Ma. morani*, and *H. calvertensis* (stem to Lipotidae + Inioidea), and *Atocetus* spp. (stem delphinoids); seven species in the analysis with equal weights, excluding *M. pappus*, *Ma. morani*, *H. calvertensis*, *B. dividus*, *P. cornutus*, and *L. calvertensis* (stem delphinidans), *T. joneti*, *Ka. serrulus*, and *W. chinookensis* (earlier branching stem to Lipotidae + Inioidea), and *Atocetus* spp. (later branching stem to Lipotidae + Inioidea). The five species of *Kentriodon* included in our second set of analyses do not form a monophyletic group in any of our trees; the most exclusive clade containing these five species also contains at least one (*R. squalodontoides*, with equal weights) to five (for example *Ka. serrulus*, *M. protohumboldti* n. gen., n. sp., *R. squalodontoides*, *T. joneti*, and *W. chinookensis*, with K = 3) other species.

It should be noted that except for some relationships (i.e. sister group relationship between *Atocetus iquensis* and *Atocetus nasalis* as well as between *Kampholophos serrulus* and *Wimahl chinookensis*), bootstrap and jackknife support values are lower than 50 for most nodes among 'kentriodontids' s.l. (Fig. 15). The proposed relationships should thus be treated with caution.

DISCUSSION AND CONCLUSIONS

The newly described early delphinidan species *Mesokentriodon protohumboldti* n. gen., n. sp., from the Middle Miocene of the southeastern Pacific, shares many general similarities in terms of cranial anatomy with *Kentriodon pernix*, from the late Early to Middle Miocene of the North Atlantic (Kellogg 1927; Godfrey & Lambert 2023), which represents the type species of the type genus of the family Kentriodontidae. That said, the former species is markedly larger than the latter (bizygomatic width at least 31 % larger than in the *K. pernix* referred specimen USNM 10670 and width of occipital condyles about 54 % larger than in the *K. pernix* holotype USNM 8060). Furthermore, close relationships of *M. protohumboldti* n. gen., n. sp. with species outside the genus *Kentriodon* (namely, *Pithanodelphis cornutus*, *Rudicetus squalodontoides*, and *Tagicetus joneti*) are recovered by some of our phylogenetic analyses. We contend that the lack of consensus for the content of the genus *Kentriodon* (see above) and the absence of clear genus-level synapomorphies (see Barnes & Mitchell 1984; Whitmore & Kaltenbach 2008; Kazár & Hampe 2014; Kimura & Hasegawa 2019; Guo & Kohno 2021; Nobile *et al.* 2024) requires authors to use special caution when placing other species, particularly those with a distinctly larger size compared to *K. pernix*, in this species-rich genus. We thus refer the new Peruvian species to a distinct, newly established genus, and anticipate that the description of more material (especially ear bones, but possibly also postcranial elements) for species either previously referred to *Kentriodon* or closely related thereof may stabilize the phylogenetic relationships and allow for a more robust diagnosis of this genus.

The close phylogenetic relationship of *M. protohumboldti* n. gen., n. sp. with *K. pernix* (and several other species of *Kentriodon*) retrieved in all our analyses allows us to identify the new species as a member of the family Kentriodontidae. The content of this clade varies broadly from one analysis to the other: in addition to five species of *Kentriodon* and *M. protohumboldti* n. gen., n. sp., *Tagicetus joneti* falls in this family in three of our analyses, and the same holds true for *Kampholophos serrulus*, *Lophocetus calvertensis*, *Pithanodelphis cornutus*, *Rudicetus squalodontoides*, and *Wimahl chinookensis* in two of the analyses run with the larger taxonomic sampling. None of the kentriodontid subfamilies (or kentriodontoid families) that have been proposed in various past studies (e.g., Barnes & Mitchell 1984; Muizon 1988b; Kazár & Grigorescu 2005; Guo & Kohno 2023) are consistently recovered in our analyses.

Higher-rank phylogenetic relationships between 'kentriodontids' s.l. and other delphinidans remain unsettled. As in several previous works (Lambert *et al.* 2017; Peredo *et al.* 2018), our favoured hypothesis is the one with part of the 'kentriodontids' s.l. (including among others *Kentriodon* spp. and *M. protohumboldti* n. gen., n. sp.) as stem delphinidans. Indeed, such a topology fills a major gap (spanning the Early to Middle Miocene) in the fossil record of delphinidans, while other topologies (i.e., those with most 'kentriodontids' s.l. recovered as more closely related to either the lipotids, inioids, or delphinoids) imply a long ghost lineage either before the crown delphinoids or before the clade including lipotids and inioids.

The new species can be distinguished from *Incacetus broggii* based on both cranial dimensions and periotic morphology,

thus revealing the presence of a second medium-size early delphinidan in the Middle Miocene P0 allomember of the Pisco Formation. More complete specimens of *I. broggii* remain to be discovered to further investigate the affinities of this poorly known species (Muizon 1988a). Proposed to forerun the full establishment of the modern Humboldt Current Ecosystem (Bosio *et al.* 2020b; Collareta *et al.* 2021b), this lower part of the Pisco Formation fills a gap between the Early Miocene Chilcatay Formation, which yielded abundant remains of *Kentriodon* sp. (Bianucci *et al.* 2018), and the Late Miocene part of the Pisco Formation, which yielded 'kentriodontid' s.l. species with a more derived morphology of the vertex (*Atocetus iquensis*) and of the rostrum (the longirostrine *Belonodelphis peruanus*) (Muizon 1988a). More prospection in P0 localities may thus further contribute to our understanding of the emergence of the different delphinidan clades as well as of their eventual success in nowadays' marine and freshwater ecosystems.

Acknowledgements
We would like to thank Giulia Bosio, Claudio Di Celma, Elisa Malinverno, and Felix G. Marx for clarifying several aspects of the early (Middle Miocene) depositional history of the Pisco Formation. For the preparation of fossil specimens, we wish to thank Yohan Despres (first steps of the preparation of MNHN.F.PPI282 and PPI283) and Walter Aguirre (MUSM4693). For granting us access to the collections and facilities under their care and/or for organizing the loan of specimens we would like to thank Ali J. Altamirano, Rodolfo Salas-Gismondi, and Rafael Varas-Malca (MUSM), Guillaume Billet (MNHN), Judith Galkin (AMNH), Dave J. Bohaska, James G. Mead, John J. Ososky, and Charles W. Potter (USNM), Stephen J. Godfrey and John R. Nance (CMM), Larry G. Barnes and Vanessa R. Rhue (LACM), Sébastien Bruaux, Cécilia Cousin, Annelise Folie, and Olivier Pauwels (IRSNB). Finally, we wish to thank the two reviewers, Hiroto Ichishima and Gabriel Aguirre-Fernández, for their constructive comments.

The first description and comparison of MNHN.F.PPI282 and PPI283 have been carried out during an internship of MO at the IRSNB during her Master 2 at Sorbonne Université-MNHN (academic year 2021-2022).

The holotype and paratype of *Mesokentriodon protohumboldti* n. gen., n. sp. were collected by CdM at the locality called 'Santa Rosa' by Muizon (1988a) with funds of the 'Action spécifique Paléontologie-Andes' of the MNHN. We acknowledge financial support under the National Recovery and Resilience Plan (NRRP), Mission 4, Component 2, Investment 1.1, Call for tender No. 104 published on 02/02/2022 by the Italian Ministry of University and Research (MUR), funded by the European Union – NextGenerationEU – Project Title: BIOVERTICES (BIOdiversity of VERTebrates In the CEnozoic Sea) – CUP I53D23002070 006 – Grant Assignment Decree No. 965 adopted on 30/06/2023 by the Italian Ministry of Ministry of University and Research (MUR).

REFERENCES

Barnes L. G. 1978. — A review of *Lophocetus* and *Liolithax* and their relationships to the delphinoid family Kentriodontidae (Cetacea: Odontoceti). *Contributions in Science, Natural History Museum of Los Angeles County* 28: 1-35.

Barnes L. G. 1985. — The Late Miocene dolphin *Pithanodelphis* Abel, 1905 (Cetacea, Kentriodontidae) from California. *Los Angeles County Museum Contributions in Science* 367: 1-27.

Barnes L. G. & Mitchell E. D. 1984. — *Kentriodon obscurus* (Kellogg, 1931), a fossil dolphin (Mammalia: Kentriodontidae) from the Miocene Sharktooth Hill Bonebed in California. *Contributions in Science, Natural History Museum of Los Angeles County* 353: 1-23.

Bianucci G. 2001. — A new genus of kentriodontid (Cetacea: Odontoceti) from the Miocene of south Italy. *Journal of Vertebrate Paleontology* 21 (3): 573-577. https://doi.org/10.1671/0272-4634(2001)021[0573:ANGOKC]2.0.CO;2

Bianucci G. 2005. — *Arimidelphis sorbinii* a new small killer whale-like dolphin from the Pliocene of Marecchia River (Central Eastern Italy) and a phylogenetic analysis of the Orcininae (Cetacea: Odontoceti). *Rivista Italiana di Paleontologia e Stratigrafia* 111 (2): 329-344.

Bianucci G. & Collareta A. 2022. — An overview of the fossil record of cetaceans from the East Pisco Basin (Peru). *Bollettino della Società PaleontoIogica Italiana* 61: 19-60. https://doi.org/10.4435/BSPI.2022.04

Bianucci G., Collareta A., Bosio G., Landini W., Gariboldi K., Gioncada A., Lambert O., Malinverno E., Muizon C. de, Varas-Malca R., Villa I. M., Coletti G., Urbina M. & Di Celma C. 2018. — Taphonomy and palaeoecology of the lower Miocene marine vertebrate assemblage of Ullujaya (Chilcatay Formation, East Pisco Basin, southern Peru). *Palaeogeography, Palaeoclimatology, Palaeoecology* 511: 256-279. https://doi.org/10.1016/j.palaeo.2018.08.013

Bianucci G., Geisler J. H., Citron S. & Collareta A. 2022. — The origins of the killer whale ecomorph. *Current Biology* 32 (8): 1843-1851. https://doi.org/10.1016/j.cub.2022.02.041

Bosio G., Malinverno E., Villa I. M., Di Celma C., Gariboldi K., Gioncada A., Barberini V., Urbina M. & Bianucci G. 2020a. — Tephrochronology and chronostratigraphy of the Miocene Chilcatay and Pisco formations (East Pisco Basin, Peru). *Newsletters on Stratigraphy* 53: 213-247. https://doi.org/10.1127/nos/2019/0525

Bosio G., Malinverno E., Collareta A., Di Celma C., Gioncada A., Parente M., Berra F., Marx F. G., Vertino A., Urbina M. & Bianucci G. 2020b. — Strontium Isotope Stratigraphy and the thermophilic fossil fauna from the middle Miocene of the East Pisco Basin (Peru). *Journal of South American Earth Sciences* 97: 102399. https://doi.org/10.1016/j.jsames.2019.102399

Bosio G., Bianucci G., Collareta A., Landini W., Urbina M. & Di Celma C. 2022. — Ultrastructure, composition, and $^{87}Sr/^{86}Sr$ dating of shark teeth from lower Miocene sediments of southwestern Peru. *Journal of South American Earth Sciences* 118: 103909. https://doi.org/10.1016/j.jsames.2022.103909

Colbert E. H. 1944. — A new fossil whale from the Miocene of Peru. *Bulletin of the American Museum of Natural History* 83: 195-216. http://hdl.handle.net/2246/389

Collareta A., Di Celma C., Bosio G., Pierantoni P. P., Malinverno E., Lambert O., Marx F. G., Landini W., Urbina M. & Bianucci G. 2021a. — Distribution and paleoenvironmental framework of middle Miocene marine vertebrates along the western side of the lower Ica Valley (East Pisco Basin, Peru). *Journal of Maps* 17 (2): 7-17. https://doi.org/10.1080/17445647.2020.1850535

Collareta A., Lambert O., Marx F. G., Muizon C. de, Varas-Malca R., Landini W., Bosio G., Malinverno E., Gariboldi K., Gioncada A., Urbina M. & Bianucci G. 2021b. — Vertebrate palaeoecology of the Pisco Formation (Miocene, Peru): glimpses into the ancient Humboldt Current ecosystem. *Journal of Marine Science and Engineering* 9 (11): 1188. https://doi.org/10.3390/jmse9111188

COLLARETA A., BOSIO G., VARAS-MALCA R., BIANUCCI G., MERELLA M., URBINA M. & DI CELMA C. 2023. — The extinct nautiloid *Aturia* in the Middle Miocene of Pacific South America: new data from the Pisco Lagerstätte of Peru. *Neues Jahrbuch für Geologie und Paläontologie, Abhandlungen* 308 (1): 23-32. https://doi.org/10.1127/njgpa/2023/1128

COMMITTEE ON TAXONOMY 2024. — List of marine mammal species and subspecies. Society for Marine Mammalogy, https://www.marinemammalscience.org, consulted on October 18, 2024.

DAWSON S. D. 1996. — A description of the skull and postcrania of *Hadrodelphis calvertense* Kellogg 1966, and its position within the Kentriodontidae (Cetacea; Delphinoidea). *Journal of Vertebrate Paleontology* 16 (1): 125-134. https://doi.org/10.1080/02724634.1996.10011290

DEVRIES T. J., GROVES L. T. & URBINA M. 2006. — A new early Miocene *Muracypraea* Woodring, 1957 (Gastropoda: Cypraeidae) from the Pisco Basin of southern Peru. *Nautilus* 120 (3): 101-105. https://www.biodiversitylibrary.org/page/35185422

DI CELMA C., MALINVERNO E., BOSIO G., COLLARETA A., GARIBOLDI K., GIONCADA A., MOLLI G., BASSO D., VARAS-MALCA R. M., PIERANTONI P. P., VILLA I. M., LAMBERT O., LANDINI W., SARTI G., CANTALAMESSA G., URBINA M. & BIANUCCI G. 2017. — Sequence stratigraphy and paleontology of the upper Miocene Pisco Formation along the western side of the lower Ica Valley (Ica desert, Peru) *Rivista Italiana di Paleontologia e Stratigrafia* 123 (2): 255-273. https://doi.org/10.13130/2039-4942/8373

FRASER F. C. & PURVES P. E. 1960. — Hearing in cetaceans: Evolution of the accessory air sacs and the structure of the outer and middle ear in recent cetaceans. *Bulletin of the British Museum (Natural History), Zoology* 7: 1-140. https://www.biodiversitylibrary.org/page/27756163

GEISLER J. H., MCGOWEN M. R., YANG G. & GATESY J. 2011. — A supermatrix analysis of genomic, morphological, and paleontological data for crown Cetacea. *BMC Evolutionary Biology* 11 (112): 1-22. https://doi.org/10.1186/1471-2148-11-112

GODFREY S. J. & LAMBERT O. 2023. — Miocene toothed whales (Odontoceti) from Calvert Cliffs, Atlantic Coastal Plain, USA, *in* GODFREY S. J. (ed.), *The Geology and Vertebrate Paleontology of Calvert Cliffs, Maryland, USA*. Vol. 107. Smithsonian Contributions to Paleobiology, Washington, D.C.: 49-186. https://doi.org/10.5479/si.1943-6688.100

GUO Z. & KOHNO N. 2021. — A new kentriodontid (Cetacea: Odontoceti) from the early to middle Miocene of the western North Pacific and a revision of kentriodontid phylogeny. *PeerJ* 9: e10945. https://doi.org/10.7717/peerj.10945

GUO Z. & KOHNO N. 2023. — An Early Miocene kentriodontoid (Cetacea: Odontoceti) from the western North Pacific, and its implications for their phylogeny and paleobiogeography. *PLoS ONE* 18 (2): e0280218. https://doi.org/10.1371/journal.pone.0280218

HEYNING J. E. 1989. — Comparative facial anatomy of beaked whales (Ziphiidae) and a systematic revision among the families of extant Odontoceti. *Contributions in Science, Natural History Museum of Los Angeles County* 405: 1-64.

ICHISHIMA H. 1995. — A new fossil kentriodontid dolphin (Cetacea; Kentriodontidae) from the Middle Miocene Takinone Formation, Hokkaido, Japan. *The Island Arc* 3: 473-485. https://doi.org/10.1111/j.1440-1738.1994.tb00126.x

ICHISHIMA H., KAWABE S. & SAWAMURA H. 2021. — The so-called foramen singulare in cetacean periotics is actually the superior vestibular area. *The Anatomical Record*: 1-8. https://doi.org/10.1002/ar.24585

ICHISHIMA H., BARNES L. G., FORDYCE R. E., KIMURA M. & BOHASKA D. J. 1995. — A review of kentriodontine dolphins (Cetacea; Delphinoidea; Kentriodontidae): systematics and biogeography. *The Island Arc* 3: 486-492. https://doi.org/10.1111/j.1440-1738.1994.tb00127.x

KAZÁR E. 2005. — A new kentriodontid (Cetacea: Delphinoidea) from the Middle Miocene of Hungary. *Mitteilungen aus dem Museum für Naturkunde Berlin, Geowissenschaftliche Reihe* 8: 53-73. https://doi.org/10.1002/mmng.200410004

KAZÁR E. & GRIGORESCU D. 2005. — Revision of *Sarmatodelphis moldavicus* Kirpichnikov, 1954 (Cetacea: Delphinoidea), from the Miocene of Kishinev, Republic of Moldavia. *Journal of Vertebrate Paleontology* 25: 929-935. https://doi.org/10.1671/0272-4634(2005)025[0929:ROSMKC]2.0.CO;2

KAZÁR E. & HAMPE O. 2014. — A new species of *Kentriodon* (Mammalia, Odontoceti, Delphinoidea) from the middle/late Miocene of Groß Pampau (Schleswig-Holstein, North Germany). *Journal of Vertebrate Paleontology* 34 (5): 1216-1230. https://doi.org/10.1080/02724634.2014.857347

KELLOGG R. 1927. — *Kentriodon pernix*, a Miocene porpoise from Maryland. *Proceedings of the United States National Museum* 69 (10): 1-55. http://hdl.handle.net/10088/15706

KIMURA T. & HASEGAWA Y. 2019. — A new species of *Kentriodon* (Cetacea, Odontoceti, Kentriodontidae) from the Miocene of Japan. *Journal of Vertebrate Paleontology*: e1566739. https://doi.org/10.1080/02724634.2019.1566739

KIMURA T. & HASEGAWA Y. 2024. — New fossil lipotid (Cetacea, Delphinida) from the Upper Miocene of Japan. *Paleontological Research* 28 (4): 1-23. https://doi.org/10.2517/PR220027

LAMBERT O., ESTEVENS M. & SMITH R. 2005. — A new kentriodontine dolphin from the Middle Miocene of Portugal. *Acta Palaeontologica Polonica* 50 (2): 239-248.

LAMBERT O., BIANUCCI G., URBINA M. & GEISLER J. H. 2017. — A new inioid (Cetacea, Odontoceti, Delphinida) from the Miocene of Peru and the origin of modern dolphin and porpoise families. *Zoological Journal of the Linnean Society* 179 (4): 919-946. https://doi.org/10.1111/zoj.12479

LAMBERT O., MUIZON C. DE, MALINVERNO E., DI CELMA C., URBINA M. & BIANUCCI G. 2018. — A new odontocete (toothed cetacean) from the Early Miocene of Peru expands the morphological disparity of extinct heterodont dolphins. *Journal of Systematic Palaeontology* 16 (12): 981-1016. https://doi.org/10.1080/14772019.2017.1359689

LAMBERT O., COLLARETA A., BENITES-PALOMINO A., DI CELMA C., MUIZON C. DE, URBINA M. & BIANUCCI G. 2021. — A new small, mesorostrine inioid (Cetacea, Odontoceti, Delphinida) from four upper Miocene localities in the Pisco Basin, Peru. *Papers in Palaeontology* 7 (2): 1043-1064. https://doi.org/10.1002/spp2.1332

MALINVERNO E., BOSIO G., GASTALDELLO M. E., PELLEGRINO L., BIANUCCI G., COLLARETA A., GARIBOLDI K., URBINA M., VILLA I. M., DI CELMA C. 2025. — The early depositional history of the Pisco Formation (Middle to Upper Miocene, Peru). *Newsletters on Stratigraphy* 58 (1): 99-123. https://doi.org/10.1127/nos/2025/0864

MARX F. G., LAMBERT O. & MUIZON C. DE 2017. — A new Miocene baleen whale from Peru deciphers the dawn of cetotheriids. *Royal Society Open Science* 4 (9): 170560. https://doi.org/10.1098/rsos.170560

MARX F. G., LAMBERT O. & UHEN M. D. 2016. — *Cetacean paleobiology*. John Wiley & Sons, Chichester, 319 p. (*Topics in Paleobiology*).

MCCURRY M. R. & PYENSON N. D. 2019. — Hyper-longirostry and kinematic disparity in extinct toothed whales. *Paleobiology* 45 (1): 21-29. https://doi.org/10.1017/pab.2018.33

MCGOWEN M. R., SPAULDING M. & GATESY J. 2009. — Divergence date estimation and a comprehensive molecular tree of extant cetaceans. *Molecular Phylogenetics and Evolution* 53 (3): 891-906. https://doi.org/10.1016/j.ympev.2009.08.018

MCGOWEN M. R., MONTGOMERY S. H., CLARK C. & GATESY J. 2011. — Phylogeny and adaptive evolution of the brain-development gene microcephalin (MCPH1) in cetaceans. *BMC Evolutionary Biology* 11 (1): 1. https://doi.org/10.1186/1471-2148-11-98

MEAD J. G. & FORDYCE R. E. 2009. — The therian skull: a lexicon with emphasis on the odontocetes. *Smithsonian Contributions to Zoology* 627: 1-248. https://doi.org/10.5479/si.00810282.627

MUIZON C. DE 1988a. — Les vertébrés fossiles de la Formation Pisco (Pérou). Troisième partie : Les Odontocètes (Cetacea, Mammalia) du Miocène. *Travaux de l'Institut français d'Études andines* 42: 1-244.

MUIZON C. DE 1988b. — Les relations phylogénétiques des Delphinida. *Annales de Paléontologie* 74: 159-227.

MURAKAMI M., SHIMADA C., HIKIDA Y., SOEDA Y. & HIRANO H. 2014. — *Eodelphis kabatensis*, a new name for the oldest true dolphin *Stenella kabatensis* Horikawa, 1977 (Cetacea, Odontoceti, Delphinidae), from the upper Miocene of Japan, and the phylogeny and paleobiogeography of Delphinoidea. *Journal of Vertebrate Paleontology* 34 (3): 491-511. https://doi.org/10.1080/02724634.2013.816720

NOBILE F., COLLARETA A., PERENZIN V., FORNACIARI E., GIUSBERTI L. & BIANUCCI G. 2024. — Dawn of the delphinidans: New remains of *Kentriodon* from the Lower Miocene of Italy shed light on the early radiation of the most diverse extant cetacean clade. *Biology* 13 (2): 114. https://doi.org/10.3390/biology13020114

OCHOA D., SALAS-GISMONDI R., DEVRIES T. J., BABY P., MUIZON C. DE, ALTAMIRANO A., BARBOSA-ESPITIA A., FOSTER D. A., QUISPE K. & CARDICH J. 2021. — Late Neogene evolution of the Peruvian margin and its ecosystems: a synthesis from the Sacaco record. *International Journal of Earth Sciences*: 1-31. https://doi.org/10.1007/s00531-021-02003-1

ORLIAC M., ORLIAC C., ORLIAC M. & HAUTIN A. 2020. — A delphinid petrosal bone from a gravesite on Ahu Tahai, Easter Island: taxonomic attribution, external and internal morphology. *MorphoMuseum* 6 (2): 1-12. https://doi.org/10.18563/journal.m3.91

PEREDO C. M., UHEN M. D. & NELSON M. D. 2018. — A new kentriodontid (Cetacea: Odontoceti) from the early Miocene Astoria Formation and a revision of the stem delphinidan family Kentriodontidae. *Journal of Vertebrate Paleontology*: e1411357. https://doi.org/10.1080/02724634.2017.1411357

PERRIN W. F. 1975. — Variation of spotted and spinner porpoise (genus *Stenella*) in the eastern Pacific and Hawaii. *Bulletin of the Scripps Institution of Oceanography University of California, San Diego La Jolla, California* 21: 1-206.

PERRIN W. F. & MYRICK A. JR 1980. — Age determination of toothed whales and sirenians, *in* Proceedings International conference on determining age of odontocete cetaceans (and sirenians) La Jolla, California, September 5-19, 1978. *Reports of the International Whaling Commission*: 1-229.

RENSBERGER J. M. 1969. — A new iniid cetacean from the Miocene of California. *University of California Publications in Geological Sciences* 82: 1-43.

ROSTON R. A., BOESSENECKER R. W. & GEISLER J. H. 2023. — Evolution and development of the cetacean skull roof: a case study in novelty and homology. *Philosophical Transactions of the Royal Society B* 378 (1880): 20220086. https://doi.org/10.1098/rstb.2022.0086

SALINAS-MÁRQUEZ F. M., BARNES L. G., FLORES-TRUJILLO J. G. & ARANDA-MANTECA F. J. 2014. — Una especie de delfín fósil (Cetacea; Delphinoidea; Kentriodontoidae) del Mioceno medio de Baja California. *Boletín de la Sociedad Geológica Mexicana* 66 (1): 145-164.

SEAGARS D. J. 1982. —Jaw structure and functional mechanics of six delphinids (Cetacea, Odontoceti) [Master thesis: San Diego State University, 179 p.

SWOFFORD D. L. 2003. — *PAUP*. Phylogenetic analysis using parsimony (*and other methods). Version 4*. Sinauer Associates, Sunderland, Massachusetts.

TRUE F. W. 1912. — Description of a new fossil porpoise of the genus *Delphinodon* from the Miocene Formation of Maryland. *Journal of the Academy of Natural Sciences of Philadelphia* 15: 165-194.

WHITMORE F. C. JR & KALTENBACH J. A. 2008. — Neogene Cetacea of the Lee Creek Phosphate Mine, North Carolina. *Virginia Museum of Natural History Special Publication* 14: 181-269.

WÜRSIG B., THEWISSEN J. G. M. & KOVACS K. M. 2018. — *Encyclopedia of Marine Mammals, third edition*. Academic Press, London, 1157 p.

Submitted on 27 March 2025;
accepted on 13 May 2025;
published on 19 February 2026.

Appendix 1. — List of characters used in the phylogenetic analyses, taken from Bianucci *et al.* (2022). https://doi.org/10.7934/P6149

Appendix 2. — Character-taxon matrix (nexus file), modified from Bianucci *et al.* (2022). https://doi.org/10.7934/P6149

Appendix 3. — Constraint tree from Bayesian analysis of molecular data applied as a backbone for the phylogenetic analyses, based on McGowen *et al.* (2009, 2011) and Geisler *et al.* (2011). https://doi.org/10.7934/P6149

Appendix 4. — Single most parsimonious tree or strict consensus tree resulting from the heuristic search with different settings, namely equal weights and implied weights with K = 3, 6, 9, and 12, for two sets of taxa, a first with 45 taxa deleted for which most of the periotic scores are lacking and a second with only 40 taxa deleted (five 'kentriodontids' s.l. added). https://doi.org/10.7934/P6149

Appendix 5. — List of genus and species names cited in the text with authorship and year.

Arimidelphis Bianucci, 2005
  Arimidelphis sorbinii Bianucci, 2005
Atocetus Muizon, 1988
  Atocetus iquensis Muizon, 1988
  Atocetus nasalis (Barnes, 1985)
Belonodelphis Muizon, 1988
  Belonodelphis peruanus Muizon, 1988
Berardius Duvernoy, 1851
Bos Linnaeus, 1758
  Bos taurus Linnaeus, 1758
Brevirostrodelphis Godfrey & Lambert, 2023
  Brevirostrodelphis dividus (True, 1912) (*Brevirostrodelphis dividum* in Godfrey & Lambert 2023, corrected here to *B. dividus* for gender agreement of species latinized adjective with genus name, following ICZN article 31.2)
Brujadelphis Lambert, Bianucci, Urbina & Geisler, 2017
  Brujadelphis ankylorostris Lambert, Bianucci, Urbina & Geisler, 2017
Cammackacetus Godfrey & Lambert, 2023
  Cammackacetus hazenorum Godfrey & Lambert, 2023
Delphinus Linnaeus, 1758
  Delphinus delphis Linnaeus, 1758
Hadrodelphis Kellogg, 1966
  Hadrodelphis calvertensis Kellogg, 1966 (*Hadrodelphis calvertense* in Kellogg, 1966, corrected here to *H. calvertensis* for gender agreement of species latinized adjective with genus name, following ICZN article 31.2)
Herbeinodelphis Godfrey & Lambert, 2023
  Herbeinodelphis nancei Godfrey & Lambert, 2023
Hippopotamus Linnaeus, 1758
  Hippopotamus amphibius Linnaeus, 1758
Incacetus Colbert, 1944
  Incacetus broggii Colbert, 1944
Inia d'Orbigny, 1834
Kampholophos Rensberger, 1969
  Kampholophos serrulus Rensberger, 1969
Kentriodon Kellogg, 1927
  Kentriodon diusinus Salinas-Márquez, Barnes, Flores-Trujillo & Aranda-Manteca, 2014
  Kentriodon hobetsu Ichishima, 1995
  '*Kentriodon*' *hoepfneri* Kazár & Hampe, 2014 (see Nobile *et al.* 2024 for comments on the systematic affinities of this species)
  Kentriodon nakajimai Kimura & Hasegawa, 2019
  Kentriodon '*obscurus*' (Kellogg, 1931) (see Nobile *et al.* 2024 for comments on the systematic affinities of this species)
  Kentriodon pernix Kellogg, 1927
  Kentriodon schneideri Whitmore & Kaltenbach, 2008
  Kentriodon sugawarai Guo & Kohno, 2021
Leptodelphis Kirpichnikov, 1954
  Leptodelphis stavropolitanus Kirpichnikov, 1954
Lophocetus Cope, 1867
  Lophocetus calvertensis (Harlan, 1842)
  Lophocetus repenningi Barnes, 1978
Macrokentriodon Dawson, 1996
  Macrokentriodon morani Dawson, 1996
Miminiacetus Godfrey & Lambert, 2023
  Miminiacetus pappus (Kellogg, 1955)
Parapontoporia Barnes, 1984
  Parapontoporia sternbergi (Gregory & Kellogg, 1927)
Pictodelphis Godfrey & Lambert, 2023
  Pictodelphis kidwellae Godfrey & Lambert, 2023
Pithanodelphis Abel, 1905
  Pithanodelphis cornutus (du Bus, 1872)
Platysvercus Guo & Kohno, 2023
  Platysvercus ugonis Guo & Kohno, 2023
Rudicetus Bianucci, 2001
  Rudicetus squalodontoides (Capellini, 1878)
Sarmatodelphis Kirpichnikov, 1954
  Sarmatodelphis moldavicus Kirpichnikov, 1954
Sophianaecetus Kazár, 2006
  Sophianaecetus commenticus (Kazár, 2005)
Sus Linnaeus, 1758
  Sus scrofa Linnaeus, 1758
Tagicetus Lambert, Estevens & Smith, 2005
  Tagicetus joneti Lambert, Estevens & Smith, 2005
Tursiops Gervais, 1855
  Tursiops truncatus (Montagu, 1821)
Westmorelandelphis Godfrey & Lambert, 2023
  Westmorelandelphis tacheroni Godfrey & Lambert, 2023
Wimahl Peredo, Uhen & Nelson, 2018
  Wimahl chinookensis Peredo, Uhen & Nelson, 2018